

Modeling and comparison of passive solar heating systems
by Robert Eugene Stotts

A thesis submitted in partial fulfillment of the requirements for the degree of MASTER OF SCIENCE in Mechanical Engineering
Montana State University
© Copyright by Robert Eugene Stotts (1980)

Abstract:
Computer models were developed to simulate and compare the thermal responses of direct gain, indirect gain, isolated gain, and natural passive solar heating systems. The performances of the direct and indirect gain models were verified using data from the passive test cells at the National Center for Appropriate Technology in Butte, Montana. A 139 m^2 (1500 ft2) home with standard insulation levels was used to compare the different types of passive solar heating systems. The collector area, thermal storage, and heating load were identical for the direct, indirect, and isolated gain systems. The natural passive system, which uses only the building and its contents for thermal storage and only south-facing windows for solar radiation collection, was simulated for several different collector areas. The largest collector area was approximately one half the area used in the other three systems. Comparisons of air temperature, auxiliary heating requirements, and solar fraction were performed for several different weather patterns, each of which had the same total insolation and the same ambient temperature variation. Each of the formal passive systems was found to supply more than half the heating needed by the home, with the direct gain system outperforming the Trombe wall (indirect gain) system for all of the weather patterns tested. The natural passive systems also provided significant solar heating, indicating that locating the normal window area present in a well insulated house on the south wall of the house results in a substantial solar fraction.

STATEMENT OF PERMISSION TO COPY

In presenting this thesis in partial fulfillment of the requirements for an advanced degree at Montana State University, I agree that the Library shall make it freely available for inspection. I further agree that permission for extensive copying of this thesis for scholarly purposes may be granted by my major professor, or, in his absence, by the Director of Libraries. It is understood that any copying or publication of this thesis for financial gain shall not be allowed without my written permission.

Signature Robert E. Stotts

Date Feb. 22, 1980

MODELING AND COMPARISON OF PASSIVE SOLAR HEATING SYSTEMS

by

ROBERT EUGENE STOTTS

A thesis submitted in partial fulfillment
of the requirements for the degree

of

MASTER OF SCIENCE

in

Mechanical Engineering

Approved:

Chairperson, Graduate Committee

Head, Major Department

Graduate Dean

MONTANA STATE UNIVERSITY
Bozeman, Montana

February, 1980

ACKNOWLEDGMENTS

The author wishes to thank Dr. R. O. Warrington and Dr. R. L. Mussulman for their help and guidance in the performance of this study. The author would also like to thank Dr. L. Palmiter of the National Center for Appropriate Technology for his valuable assistance in the validation of the computer models.

This study was supported by the Engineering Experiment Station at Montana State University, Bozeman, Montana.

TABLE OF CONTENTS

	Page
VITA	ii
ACKNOWLEDGMENTS	iii
LIST OF TABLES	v
LIST OF FIGURES	vi
NOMENCLATURE	viii
ABSTRACT	xii
CHAPTER I. INTRODUCTION	1
CHAPTER II. ANALYTICAL MODELS	7
Direct Gain Model	7
Isolated Gain Model	23
Trombe Wall Model	27
Model Validation	36
CHAPTER III. RESULTS	42
CHAPTER IV. CONCLUSIONS	64
APPENDICES:	
A. SELECTION CRITERIA FOR LOCATION OF PROJECTED POINTS	67
B. DETERMINATION OF THE SUNLIT AREA CONFIGURATION	70
C. DIFFERENTIAL ELEMENT VIEW FACTORS	73
D. NUMERICAL DOUBLE INTEGRATION	77
E. INSOLATION AND AMBIENT TEMPERATURE DATA GENERATION	79
LITERATURE CITED	85

LIST OF TABLES

Table		Page
2.1	Equations for the Coordinates of Point Q_p	10
2.2	Coordinates of the Window Corner Points	10
3.1	Physical Parameters of the Passive Solar Systems	46
3.2	Auxiliary Heating and Solar Fractions for the Test Case Simulations	62
B.1	Possible Configurations of the Sunlit Areas	71
E.1	Degree Day/Night Averages for Bozeman, Montana (1968-1977)	83

LIST OF FIGURES

Figure		Page
2.1	Configuration and Nomenclature of the Direct Gain System	8
2.2	One Possible Shape for the Sunlit Areas	12
2.3	Arbitrary Planar Surfaces and Coordinate System for View Factor Determination	15
2.4	Flow Chart for the Direct Gain Model	22
2.5	The Isolated Gain System	23
2.6	Trombe Wall System and Principal Modes of Heat Transfer	29
2.7	Node Configuration for the Storage Wall Solution	34
2.8	Direct Gain Validation	38
2.9	Trombe Wall Validation	40
3.1	Direct-Indirect Gain Comparison Without Auxiliary Heating, Case I.	48
3.2	Direct-Indirect Gain Comparison Without Auxiliary Heating, Case II.	49
3.3	Natural Passive Air Temperature Without Auxiliary Heating, Case I.	50
3.4	Natural Passive Air Temperature Without Auxiliary Heating, Case II.	51
3.5	Direct-Indirect Gain Comparison with Auxiliary Heating, Case I.	53
3.6	Direct-Indirect Gain Comparison with Auxiliary Heating, Case II.	54
3.7	Natural Passive Air Temperature with Auxiliary Heating, Case I.	56

Figure		Page
3.8	Natural Passive Air Temperature with Auxiliary Heating, Case II.	57
3.9	Isolated Gain Building Air Temperature with Auxiliary Heating, Case I.	58
3.10	Isolated Gain Building Air Temperature with Auxiliary Heating, Case II.	59
C.1	Differential Element for Perpendicular Surfaces	75
C.2	Differential Element for Parallel Surfaces	76
E.1	The Assumed Insolation Distribution	80
E.2	The Assumed Ambient Temperature Distribution	82

NOMENCLATURE

Symbol	Description
a	distance from Z axis to window edge (see Figure 2.2)
A	Area
A_v'	vent area per unit width of storage wall (indirect gain)
b	distance from Y axis to window edge (see Figure 2.2)
b	storage wall thickness (indirect gain)
c	specific heat
c_p	specific heat at constant pressure (air)
C_a	Y-coordinate of arbitrary point Q (see Figure 2.1)
C_b	Z-coordinate of arbitrary point Q (see Figure 2.1)
C_d	vent discharge coefficient
DD	heating degree days, as defined by Equation (E.5)
DL	day length (hours)
DN	heating degree nights, as defined by Equation (E.7)
f(x)	initial storage wall temperature distribution
F_{A-B}	diffuse radiation view factor for radiation from surface A to surface B
g	acceleration due to gravity
Gr	Grashof number = $g\beta(T_w - T_\infty)x^3/\nu^2$
h	window height (see Figure 2.2)
h	heat transfer coefficient
$\bar{h}$	average heat transfer coefficient

Symbol	Description
h_0	heat transfer coefficient on window side of storage wall
h_b	heat transfer coefficient on interior side of storage wall
H	room height (see Figure 2.1)
H	storage wall height (indirect gain)
HS	daily total insolation
J	radiosity (total radiation which leaves a surface per unit time per unit area)
k	thermal conductivity of storage wall
l	window length (see Figure 2.2)
L	room length (see Figure 2.1)
m	mass
$\dot{m}$	mass flow rate of air
n	number of nodes in storage wall
$\overline{Nu}$	average Nusselt number = $\frac{\overline{h}L}{k}$
Pr	Prandtl number = $\frac{c_p \mu}{k}$
q_{ave}	average (numerical) solar flux, as defined by Equation (E.3)
q_s	solar flux, as defined by Equation (E.4)
Q_r	net total long-wavelength radiant heat transfer rate to a surface
Q_s	total absorbed insolation (rate)
r	infiltration rate (air changes per hour)
R	thermal resistance factor
SR	time of sunrise = $12 - \frac{DL}{2}$

Symbol	Description
SS	time of sunset = $12 + \frac{DL}{2}$
t	solar time (hours)
T	temperature (absolute)
T_{amb}	ambient temperature
T_{max}	daily maximum ambient temperature (see Figure E.2)
T_{mean}	average (numerical) ambient temperature, as defined by Equation (E.10)
T_{out}	vent outlet temperature (see Figure 2.6)
T_{space}	average air space temperature (see Figure 2.6)
T_w	storage wall temperature distribution
U	over-all heat transfer coefficient
UA_{tot}	heating load
W	room width (see Figure 2.1)
x	coordinate
y	coordinate
z	coordinate
α	surface azimuth angle of insolation (see Figure 2.1)
α	thermal diffusivity = $\frac{k}{\rho c}$
β	elevation angle of insolation (see Figure 2.1)
β	thermal expansion coefficient
γ	elevation angle of insolation, as projected onto X-Z plane (see Figure 2.2)
Δt	time step

Symbol	Description
Δx	node spacing (see Figure 2.7)
ε	long-wavelength radiation emittance
λ	dimensionless parameter, as defined by Equation (2.34)
μ	dynamic viscosity
ν	kinematic viscosity = $\frac{\mu}{\rho}$
ρ	density
σ	Stefan-Boltzmann constant = $5.669 \times 10^{-8} \frac{W}{m^2 \circ K^4}$

Subscripts

air	direct gain system air
i	surface (direct gain)
i	storage wall node
int	all interior surfaces except storage wall (lumped)
p	projection (in the insolation direction)
room	room air (indirect and isolated gain)
wall	storage wall
win	window
y	Y-coordinate

Superscripts

'	at the next time

ABSTRACT

Computer models were developed to simulate and compare the thermal responses of direct gain, indirect gain, isolated gain, and natural passive solar heating systems. The performances of the direct and indirect gain models were verified using data from the passive test cells at the National Center for Appropriate Technology in Butte, Montana. A 139 m^2 (1500 ft^2) home with standard insulation levels was used to compare the different types of passive solar heating systems. The collector area, thermal storage, and heating load were identical for the direct, indirect, and isolated gain systems. The natural passive system, which uses only the building and its contents for thermal storage and only south-facing windows for solar radiation collection, was simulated for several different collector areas. The largest collector area was approximately one half the area used in the other three systems. Comparisons of air temperature, auxiliary heating requirements, and solar fraction were performed for several different weather patterns, each of which had the same total insolation and the same ambient temperature variation. Each of the formal passive systems was found to supply more than half the heating needed by the home, with the direct gain system outperforming the Trombe wall (indirect gain) system for all of the weather patterns tested. The natural passive systems also provided significant solar heating, indicating that locating the normal window area present in a well insulated house on the south wall of the house results in a substantial solar fraction.

CHAPTER I

INTRODUCTION

Solar heating systems are receiving ever-increasing attention as alternate means of space heating. This is due to the spiraling costs of conventional (electric, gas, and oil) heating. Two basic types of solar heating systems, active and passive, are available. Active systems are characterized by collectors, pumps or fans, and elaborate heat delivery systems, such as plumbing or vents. They require a large initial capital investment and may require extensive maintenance. Control systems to regulate heat delivery to the building add to the complexity of these systems.

A passive solar heating system, on the other hand, is, by its very nature, an integral part of the building it heats. Passive systems consist of a large window (contained in the building's walls) for solar radiation collection and some means of thermal storage. The storage is usually a masonry material, such as bricks or concrete, or consists of water-filled containers. If the storage is distributed about the room containing the window, the system is referred to as a direct gain system. The thermal storage of indirect gain systems is concentrated into a wall a short distance from the window. This wall prevents most or all of the sunlight from entering the living space. Isolated gain systems are passive systems in which the collection and storage components are thermally isolated from the living space. A means of transferring heat from the storage to the living space, such as a fan, is necessary. One

example of this type of system is a solar greenhouse. Natural passive systems are direct gain systems with no added storage, other than the normal contents of the building. Thermal storage is only in the house itself and in its contents. Passive systems typically do not efficiently regulate heat delivery to their buildings. All the aforementioned passive systems, except the isolated gain types, rely on the thermal interactions between the various components of the system (window, storage and the building itself) to control the air temperature. During daylight hours, the large amounts of incident solar radiation (insolation) which pass through the window are mostly absorbed by the storage. This moderates peak daytime temperatures. At night, convection and radiation from the storage supply heat to the building. Since these interactions are functions of many variables (including the building heating characteristics, amount and type of storage, window area and type, and the ambient conditions), large air temperature fluctuations may occur. Indirect gain systems typically exhibit lower air temperature fluctuations than do direct gain or natural passive systems. Natural passive systems experience the largest fluctuations, due to their relatively small thermal storage. Isolated gain systems control the building air temperature much better than other types of systems, but high temperatures may occur within the collector.

Since passive systems are integral parts of the buildings they heat, they are not normally retrofitted. Instead, the storage and

window are incorporated into the building during original construction, often using the storage for structural support. In order to properly size the window area and storage for the system, some means of predicting its long-term performance, before it is built, is desirable. Rule-of-thumb methods are available to size the window area and the thermal storage [1]. However, these methods will not accurately (within 10%) predict the actual performance of the system. They are, however, useful for making a first guess.

Two other methods are also available for making an accurate prediction of the performance of passive systems. The first method is the use of computer models of the passive systems. The models are developed using basic thermodynamic and heat transfer equations to approximate the thermal response of the systems. F. Trombe [2] performed the first comprehensive modeling of the passive solar system commonly known as the Trombe wall system. It is an indirect gain system which uses a masonry wall, with vents at the top and bottom, for storage. Air flow from the living space through the vents transfers heat, by natural convection, to the living space. Extensive modeling of this system has been performed [3,4,5]. Several of these models were used to optimize various components of the Trombe wall system. Many of these models are also applicable to water wall systems. They are indirect gain systems which use water-filled containers for the storage wall. Models have also been developed to simulate the performance of direct gain systems [6,7]. The

first of these is a simple general model which is applicable to any type of passive system. The other is a model whose complexity rivals that of the direct gain model developed for this study. The model for this study was derived from basic principles. Little modeling has been done for natural passive and isolated gain systems.

When a passive solar system model is developed, some means of testing its performance is needed. This is usually done by using the model to simulate the experimentally measured performance of a system of the modeled type. Passive test cells are currently in use in several parts of the country to obtain the necessary data [8,9]. Some of this data was used to verify the performance of two of the models which were developed for this study. Models were developed to simulate the performance of direct, indirect (Trombe wall) and isolated gain systems. The direct gain model was also used to simulate the performance of natural passive solar systems.

The other method which is currently available to predict the performance of passive systems is a simplified method developed by Balcomb et al [10], at the Los Alamos Scientific Laboratories (LASL). The method is applicable to Trombe wall, water wall and direct gain systems. It estimates the performance of the systems as a function only of the building heating load, the monthly absorbed insolation and the total monthly heating degree days for the location of interest. Two additional climatic factors could be used to improve the method. The first

factor is the modification of degree days into degree days for daytime ambient temperatures and degree nights for nighttime ambient temperatures (see Appendix E). This modification has already been shown to increase the accuracy of simulations [11]. The second factor is a cloudy/clear day factor (CCDF). It would account for the differences in clear and cloudy day groupings for different geographical locations. The performance of all passive systems is dependent on the grouping of clear and cloudy days which occurs. The dependency on the CCDF is not yet known, but the simulations which were performed for this study represent the first step in determining this dependence. Simulations were performed for the various modeled systems (direct gain, indirect gain, isolated gain, and natural passive) for two different clear and cloudy day groupings. The natural passive system was simulated for two different window areas. The first approximated the normal window area present in a residence. The windows were assumed to all be on the south side of the building so that they could all provide solar heating. The second window area was approximately one half the window area present in the three formal passive systems. The window area, storage and heating load were identical for the three. The simulations formed a basis for a comparison of the performance of the four systems, for the two test cases. Comparisons of direct gain and Trombe wall systems have already been performed [12,13]. Direct gain systems without night window insulation were found to perform better (economically) than Trombe

wall systems with night window insulation in southern U.S. climates. However, Trombe wall systems with night insulation were found to be more economical that direct gain systems with night insulation in northern U.S. climates. None of these studies includes isolated gain or natural passive systems. Since data for verification of these two models were not available, the results of their simulations are only preliminary and should be treated accordingly.

CHAPTER II

ANALYTICAL MODELS

The differential equations which were used to develop the passive solar system models were obtained from basic principles. Basic thermodynamic laws were combined with theoretical and empirical heat transfer equations. A few simplifying assumptions were used to reduce the complexity of the problems.

Direct Gain Model

This model was developed for a single room with a single window. It could, however, be easily expanded to model a more complex building, such as an entire dwelling. To obtain high accuracy and generality, all modes of heat transfer within the room were assumed to be important. Radiative exchange among the walls, floor, ceiling, and window was incorporated into the model. Convection from each surface in the room to the room air and conduction from these surfaces, through the walls, to the ambient were also computed. The desired degree of accuracy necessitated knowing the size, location and shape of the sunlit areas within the room. This resulted in a complex geometry problem.

Figure 2.1 illustrates the geometry of the modeled direct gain system. Sunlight enters the room through the window at an elevation angle β and a surface azimuth angle α. Morning sun has a positive α. The entering sunlight may fall, in part or in full, on the floor or on any of the north, west, and east walls. For this model, the sunlit portion

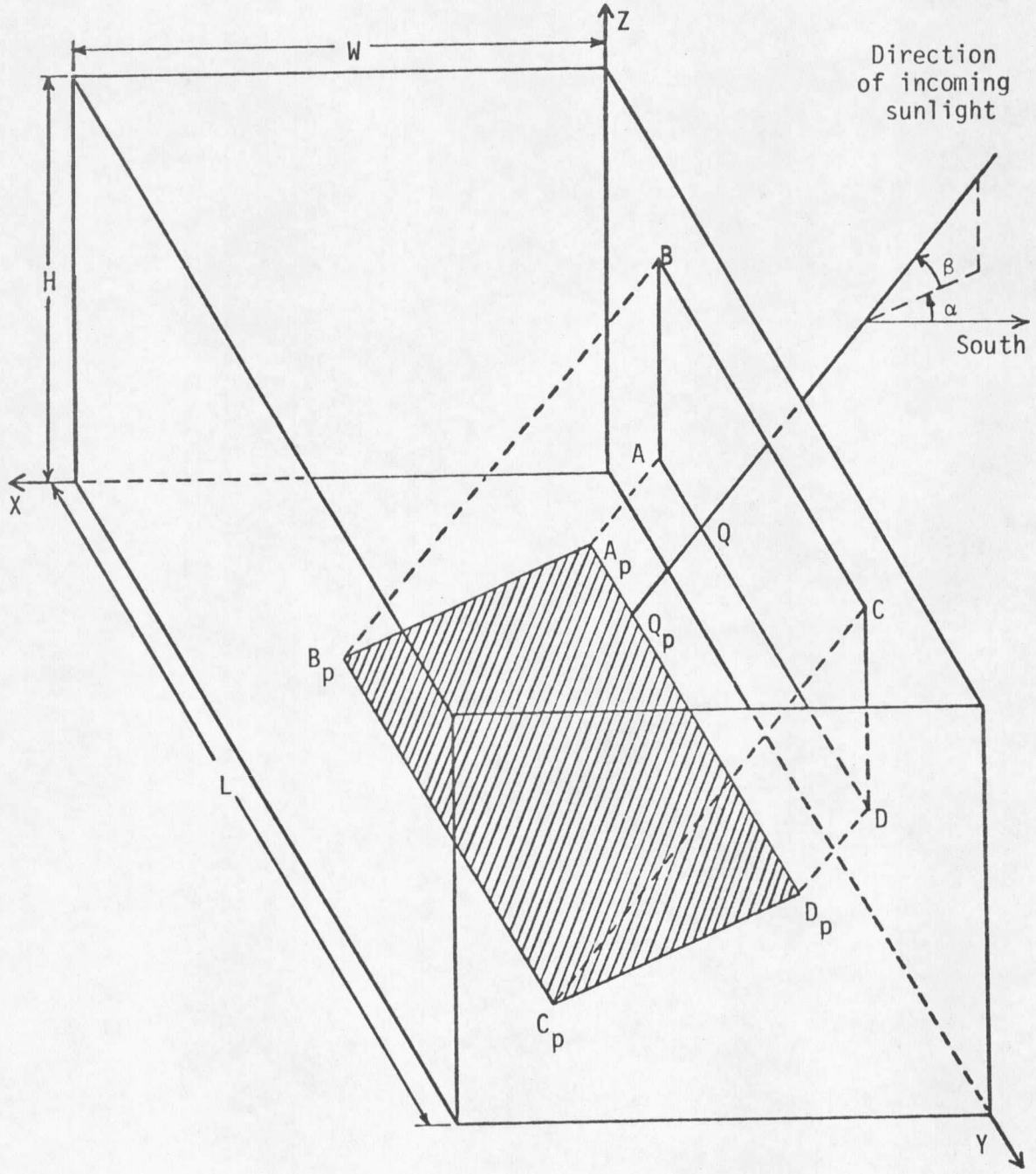


Figure 2.1 Configuration and Nomenclature of the Direct Gain System

of each of these surfaces was treated as an individual surface.

During the course of a normal day, the size, location and shape of the sunlit areas within the room change continuously. These are functions only of the room geometry and the direction of the incident solar radiation (insolation). The direction of the insolation (α and β) was calculated using relations from Duffie and Beckman [14]. These angles are functions only of the window orientation (azimuth angle and slope), the latitude, the time of day and the day of the year. Provision was made in the model for a non-vertical, non-south-facing window.

Once the insolation direction was known, the size, location and shape of the sunlit areas were found. The first step in this was to locate the projections (in the direction of the insolation) of the corner points of the window. For example, consider any point Q on the south wall of the room, as shown in Figure 2.1. The coordinates of point Q are $(0,C_a,C_b)$. Expressions for the coordinates of its projection, Q_p, are given in Table 2.1, as a function of where the projected point falls. In these equations, the angle γ (see Figure 2.2) is defined as

$$\gamma = \tan^{-1}(\tan \beta/\cos \alpha). \qquad (2.1)$$

Obviously, with four different sets of equations for the coordinates of Q_p, some means of determining which surface the point intersected was needed. One method of accomplishing this determination would be to

Table 2.1 Equations for the Coordinates of Point Q_p

Coordinate	Q_p falls on the floor	north wall	west wall	east wall	Limits
X	$C_b \cot\gamma$	W	$(L - C_a)\cot\alpha$	$-C_a\cot\alpha$	$0 \leq X \leq W$
Y	$C_a + C_b \tan\alpha \cot\gamma$	$C_a + W\tan\alpha$	L	0	$0 \leq Y \leq L$
Z	0	$C_b - W\tan\gamma$	$C_b - (L-C_a)\tan\gamma\cot\alpha$	$C_b + C_a \tan\gamma \cot\alpha$	$0 \leq Z \leq C_b$

Table 2.2 Coordinates of the Window Corner Points

Corner Point	Coordinates
A	(0,a,b)
B	(0,a,b+h)
C	(0,a+l,b+h)
D	(0,a+l,b)

calculate the coordinates of the projected point with each of the sets of equations and compare the results of each set with the allowable limits of each coordinate. The limits are listed in Table 2.1. The selection criteria were based on this method, but were condensed into a smaller set of inequalities which, when satisfied, determined the location of the projected point. These selection criteria are given in Appendix A. The projections of the window corner points were found using this method. The coordinates of the corner points (to be used in the equations in Table 2.1) are given in Table 2.2.

After locating A_p, B_p, C_p, and D_p, the size, shape and location of the sunlit areas were calculated. There were 19 possible configurations for the sunlit areas. These possibilities were designated by the set of locations of the projected window corner points. For example, one such set is {A_p, B_p, and D_p on the floor and C_p on the west wall}. This configuration is illustrated in Figure 2.2. The shaded areas represent the sunlit portions of the room. Appendix B contains a list of all the possible configurations that the sunlit areas may assume. Also included is a brief description of the method which was used to determine which configuration occurred for any insolation direction.

It is apparent from Figure 2.2 that the sunlit areas in the room have complex geometrical shapes which change continuously throughout the day. For this reason, and since diffuse radiation view factors are difficult to calculate for odd shapes, an equivalent rectangle was

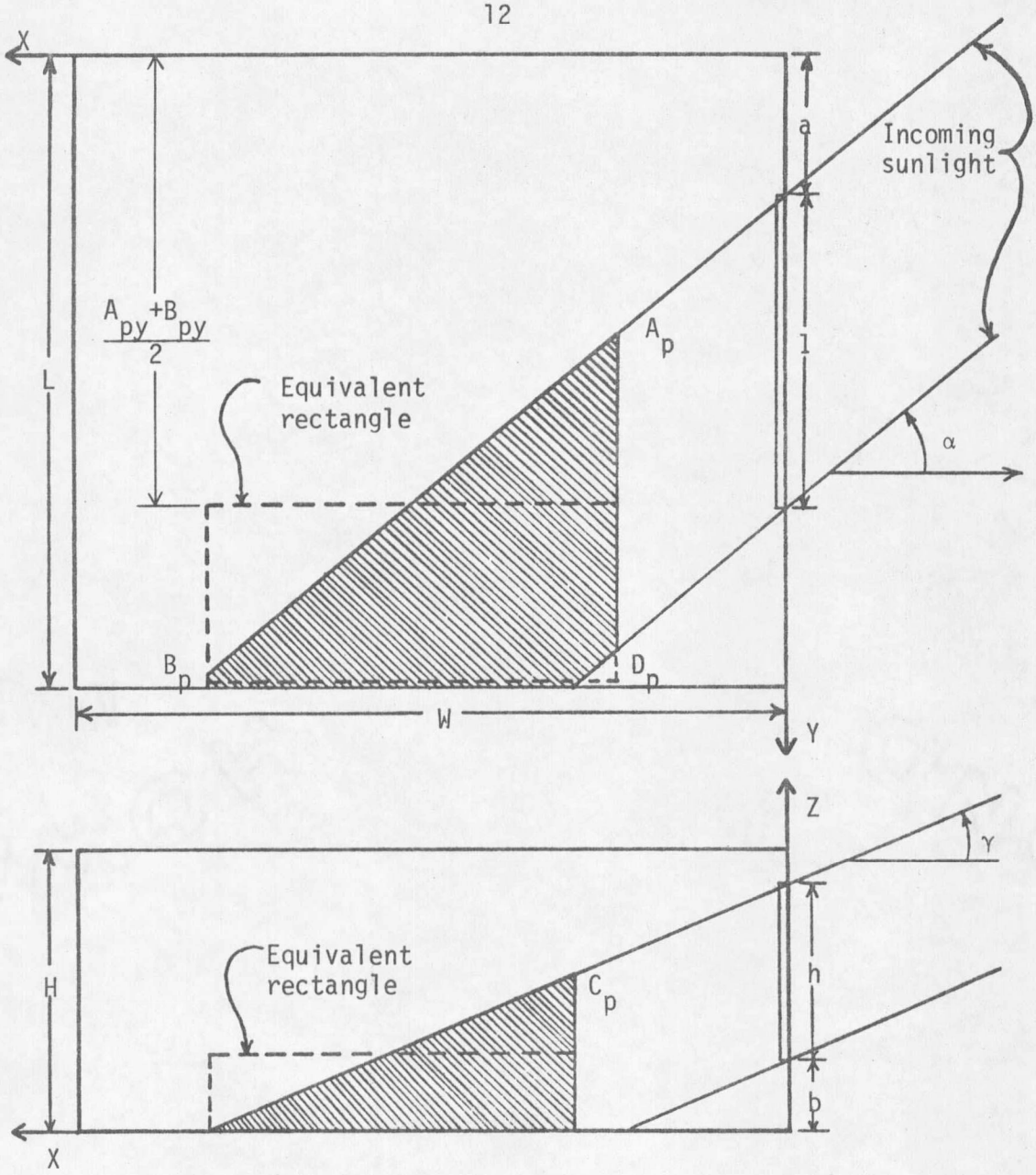


Figure 2.2 One Possible Shape for the Sunlit Areas

generated for each sunlit area within the room. Each rectangle had the same area and approximately the same location as the sunlit area it represented. As many edges as possible of the rectangle coincided with the corresponding edges of the sunlit area. Figure 2.2 illustrates the equivalent rectangles for one possible configuration.

The fraction of the insolation passing through the window incident on each sunlit surface was also determined. This was calculated by dividing the actual sunlit area by the sunlit area which would occur if the wall (or the floor) was large enough to accomodate all the insolation. This calculation, and all the preceding ones, were performed using only the room dimensions, α, β and the coordinates of A_p, B_p, C_p, and D_p. The coordinates of the projected window corner points were used whenever possible in order to simplify the derivation of the equations. Each of the 19 possible configurations has its own set of equations, but due to space restrictions, the equations are not presented here.

The transmissivity of the glazing (window) was calculated, as a function of the incidence angle and the number of window panes, using the method suggested by Duffie and Beckman for flat plate solar collectors [14]. Once the amount and location of the insolation entering the room was known, the solar radiation absorbed by each surface, Q_{si}, was estimated. Each sunlit area was assumed to absorb a fraction, equal to its solar absorptivity, of the insolation incident on it. The reflected sunlight was assumed to be totally diffuse and to be distributed over

the entire inside surface of the room.

In this model, radiative heat exchange among the sunlit areas, walls, floor, ceiling, and window was assumed to contribute significantly to the total thermal response of the room. In order to determine the net radiative transfer among the various surfaces, the diffuse radiation view factors must be known for each pair of heat transfer surfaces. Consider any two flat surfaces, such as those shown in Figure 2.3. If the view factor from dA_1 to A_2, F_{d1-2}, is known as a function of x and y, then F_{2-1} is given by

$$F_{2-1} = \frac{1}{A_2} \int_0^b \int_0^a F_{d1-2} \, dx \, dy. \qquad (2.2)$$

Appendix C contains the various expressions which were used for F_{d1-2} in this model. The view factor F_{2-1} could be determined exactly by performing the integral shown in Equation (2.2). However, the expressions for F_{d1-2} are often very complex (see Appendix C) and are not easily integrated. For this reason, a numerical method was used to perform the necessary double integration. The numerical double integration scheme which was used in this model appears in Appendix D.

Using an approach similar to that presented by Holman [15], the equations governing steady radiative heat transfer among the surfaces in the room were found to be

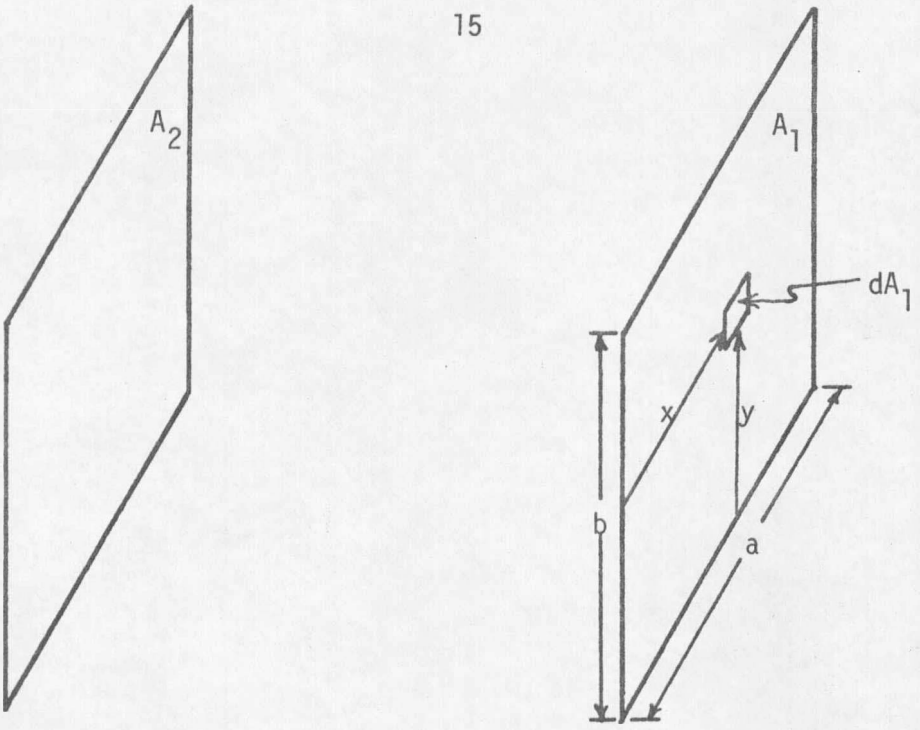


Figure 2.3 Arbitrary Planar Surfaces and Coordinate System for View Factor Determination

$$\frac{\sigma T_i^4 - J_i}{1 - \varepsilon_i} \varepsilon_i A_i + \sum_{j=1}^{11} (J_j - J_i) A_j F_{ji} = 0 \qquad (2.3)$$

for i = 1,2,3,...,11. The first term represents the net thermal radiation leaving surface i. Each term in the summation represents the net radiative heat transfer from surface j to surface i. For steady radiation, the sum of all these terms (including the first term) must equal zero. This set of equations was solved for {J} using Gaussian elimination. Knowing {J}, the net (long wavelength) radiative heat transfer rate to each surface, Q_{ri}, was found, using

$$Q_{ri} = (J_i - \sigma T_i^4) \frac{\varepsilon_i A_i}{1 - \varepsilon_i} . \qquad (2.4)$$

In this model, the room air was assumed to be transparent to solar and thermal radiation [16]. Because of this assumption, heat may only be transferred to the room air by conduction and/or convection. To account for both modes, heat transfer coefficients were used. Some means of determining a heat transfer coefficient for each surface in the room was thus needed.

In any sunlit room, the portion of the walls and the floor on which sunlight falls directly was expected to heat up to a temperature higher than the temperature of either the air or of the non-sunlit surfaces in the room. This temperature differential could cause significant air movements in the room, especially if the sunlit portion is large. This air movement could affect all the air in the room, significantly increasing the total convective heat transfer to the room air. However, since all methods available for accounting for the air movement are very complicated, and since no simple empirical method is available to estimate this effect, it was neglected. Instead, the air movements were assumed to result in complete (perfect) mixing of the room air.

Much work has been done developing empirical relations for determination of heat transfer coefficients for natural convection from surfaces to semi-infinite fluids [15]. These relations are usually written in the dimensionless form

$$\overline{Nu} = \frac{\bar{h}L}{k} = C(GrPr)^m, \qquad (2.5)$$

and account for both conduction and convection, since they are experimentally determined. C and m are dimensionless parameters dependent on the surface shape and orientation and on the degree of turbulence present in the flow, which is, in turn, dependent on the magnitude of the Grashof-Prandtl number product (Rayleigh number). The fluid properties used in Equation (2.5) are normally determined at the film temperature. The film temperature is the average of the fluid and the heat transfer surface temperatures. Equation (2.5) was used in this model to estimate the heat transfer coefficient, h_i, for each surface. Each was assumed to interact with the room air independent of all other surfaces in the room. The values for C and m were obtained from Holman [15].

In addition to convection to the room air, each surface in the room was also assumed to interact with the ambient and to store thermal energy. The heat loss from each surface to the ambient was written in terms of the effective thermal resistance between the surface and the ambient. The thermal storage of each surface was assumed to be concentrated in the first physical layers of the wall, before the insulation. For example, consider a wall constructed of 2" x 4" wooden studs with fiberglass insulation between the studs and with an inside surface of 1/2" gypsum board (sheet rock). The construction of the outside surface of the wall is unimportant for storage considerations. The thermal storage would be

concentrated in the gypsum board and the sheet rock would be treated (excluding the sunlit portion of the wall) as an isothermal body.

In this model, the room's interior surface was divided into 11 surfaces. Surfaces one through four were, respectively, the non-sunlit portions of the floor and of the north, west, and east walls. Surface five was the south wall (less the window) and six was the ceiling. Surfaces seven through ten were, respectively, the sunlit portions of the floor and the north, west, and east walls. Surface eleven was the inside pane of the window. Each of these surfaces was treated as an individual lumped-capacity system.

The differential equations governing the thermal response of the various surfaces in the room were derived by performing a heat balance on each surface. The heat balance was of the form

[Solar radiation absorbed] + [net thermal radiation from other surfaces] - [convection to the room] - [loss to the ambient] = [storage].

Substituting the appropriate mathematical expressions for each term resulted in the set of (11) differential equations

$$Q_{si} + Q_{ri} - h_i A_i (T_i - T_{air}) - A_i (T_i - T_{amb})/R_i = (mc)_i \frac{dT_i}{dt} . \qquad (2.6)$$

The corresponding initial conditions for these equations were

$$T_i)_{t=0} = T_{0i} \tag{2.7}$$

The two radiation components (solar and thermal) were treated independently because most common construction materials have very different absorptances for the two types. For example, a normal white paint has a solar absorptance between 0.3 and 0.5. The same paint, however, has an emittance (at 25°C) between 0.85 and 0.95 [17].

The differential equation for the room air was derived using a similar approach. The heat balance was of the form

[convection from surfaces] - [infiltration] = [storage].

The corresponding mathematical expressions were substituted into this balance, and the resultant differential equation was

$$\sum_{i=1}^{11} A_i h_i (T_i - T_{air}) - r(mc)_{air}(T_{air} - T_{amb}) = (mc)_{air}\frac{dT_{air}}{dt}. \tag{2.8}$$

The initial condition for the air was

$$T_{air})_{t=0} = T_{0air}. \tag{2.9}$$

In Equation (2.8), r is the infiltration rate in air changes per hour.

Equations (2.6) through (2.9) were solved numerically using a forward-stepping, explicit finite difference method. The approximation

$$\frac{dT}{dt} = \frac{T' - T}{\Delta t} + O[\Delta t] \tag{2.10}$$

was substituted into Equations (2.6) and (2.7) and the resultant equations were solved for T'. The set of explicit equations to determine the new surface temperatures was found to be

$$T_i' = [Q_{si} + Q_{ri} + h_i A_i T_{air} + A_i T_{amb}/R_i]\frac{\Delta t}{(mc)_i} + [1 - \frac{\Delta t A_i}{(mc)_i}(h_i + 1/R_i)]T_i. \quad (2.11)$$

The resulting explicit expression for the new air temperature was

$$T'_{air} = \frac{\Delta t}{(mc)_{air}} \left\{ \sum_{i=1}^{11} A_i h_i T_i + r(mc)_{air} T_{amb} + [\frac{(mc)_{air}}{\Delta t} - \sum_{i=1}^{11} A_i h_i - r(mc)_{air}]T_{air} \right\}. \quad (2.12)$$

In order to guarantee stability of the numerical method, the coefficients of T_i in Equations (2.11) and of T_{air} in Equation (2.12) must be non-negative [18]. This restriction forced the following restrictions on the time step, Δt:

$$\Delta t \leq \frac{(mc)_i/A_i}{(h_i + 1/R_i)} \quad (2.13)$$

and

$$\Delta t \leq \frac{(mc)_{air}}{\sum_{i=1}^{11} h_i A_i + (mc)_{air} r}. \quad (2.14)$$

All of the preceding equations were incorporated into a computer

code to simulate the thermal response of the direct gain system. Figure 2.4 illustrates the programming logic which was used for this model. This flowchart, though greatly simplified, shows the essential features of the logic. The most complicated and the longest portion on the model was the subroutine which calculated the geometric parameters (including the radiation view factors). Each time the view factors were recalculated, many (up to 55) numerical double integrations were performed. It was estimated that this part of the model required more than 75% of the total cpu time needed for each run.

In this model, the radiative heat transfer to each surface (solar and thermal) was calculated only once for each set of data. This procedure resulted in limitations on the time step between successive data sets (DT). These limitations were found, during the model verification procedure, to be 0.25 hours during high insolation periods (i.e. during the day) and to be 0.50 hours at night. The model could be modified to accept hourly data simply by altering the computer code to recalculate the radiative heat transfer rates several (four or more) times per data step. The maximum time step (DELT), which was used to calculate the new temperatures, was found using Equations (2.13) and (2.14). A time step equal to 99% of the maximum allowable was used to avoid instability due to computer round-off error, yet still obtain the fastest possible computation time.

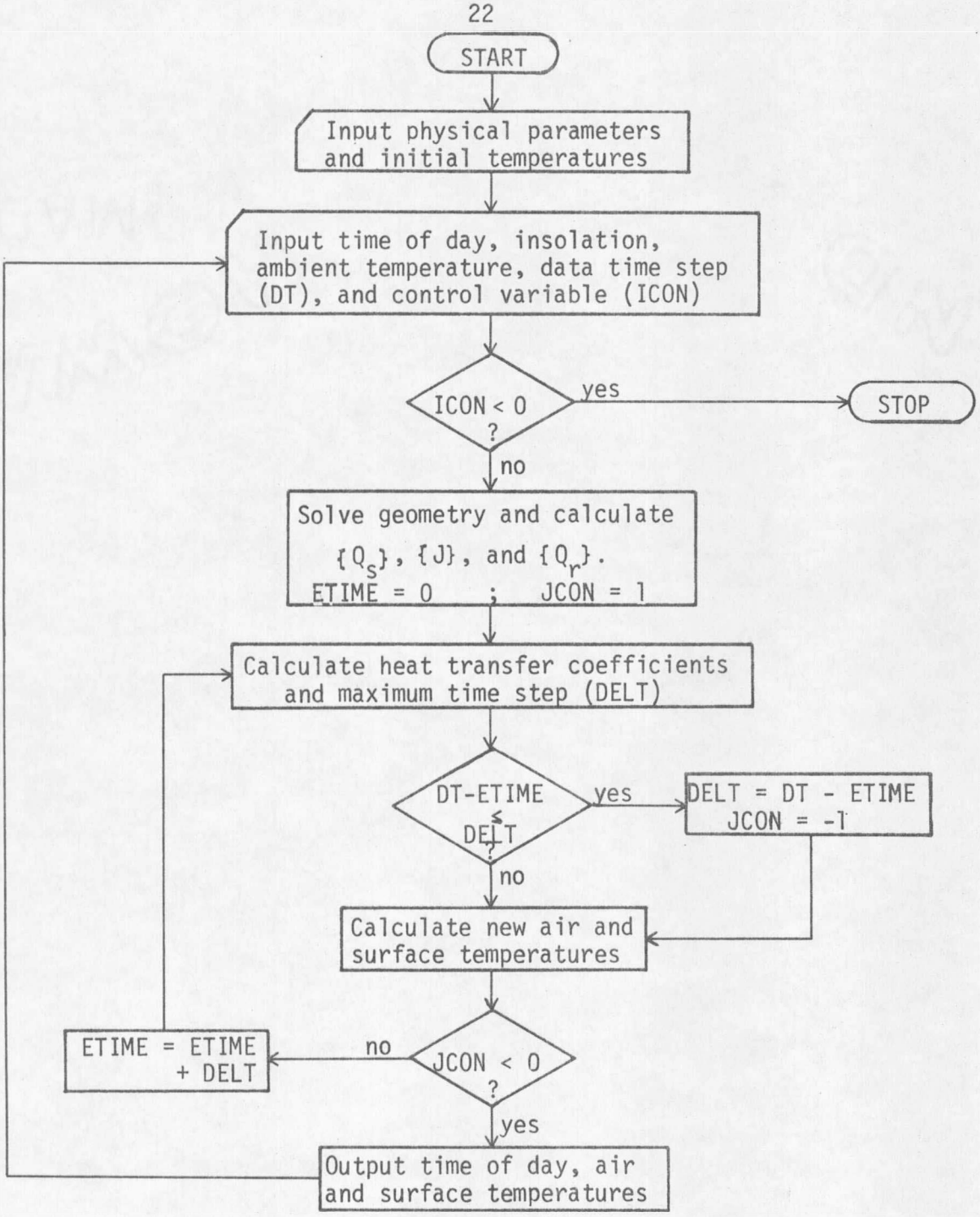


Figure 2.4 Flow Chart for the Direct Gain Model

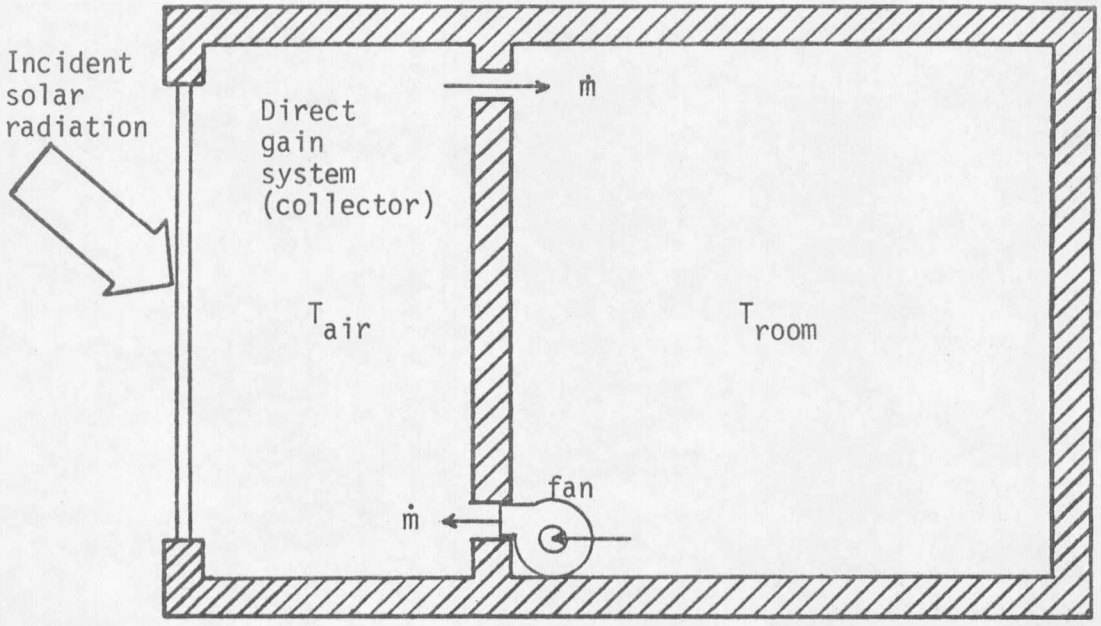


Figure 2.5 The Isolated Gain System

Provision was also made in this model for nighttime collector window insulation. Whenever the insolation dropped to zero, the thermal resistance of the window, R_{11}, was increased by the R-factor of the window insulation. This R-factor may be any desired value. When the insolation again became non-zero, R_{11} was reduced to its original value.

Isolated Gain Model

An isolated gain passive solar system is any passive system in which the collection and storage areas are thermally isolated from the building that the system is intended to heat (for example, a solar greenhouse). A model for isolated gain was developed using a direct gain system attached to a building, as illustrated in Figure 2.5. The building

and the collector (the attached direct gain system) were assumed to have one common wall, the north wall of the collector. A fan provided air exchange between the building and the collector.

It was obvious that any model for this type of isolated gain system should be based on the direct gain model. Because of the similarity of the systems, the direct gain model was used, with a few modifications, to model the thermal response of an isolated gain system of the type shown in Figure 2.5. It is apparent that the geometry of the attached direct gain system would be unchanged. The radiative heat exchange equations for the collector were also not changed by its addition to the building. The convective heat transfer from the various surfaces in the collector to the collector air was affected by the large air movements caused by the fan. However, like the thermal air currents, it is difficult to account for this effect. Because of this difficulty, the air movements caused by the fan were assumed to result in perfect mixing of the collector air. Conduction from the surfaces in the room through their corresponding walls was the same for all surfaces except numbers two and eight (north wall surfaces). Heat transfer from these surfaces was to the building air, rather than to the ambient. To account for this difference, Equations (2.6) and (2.11) were modified. For i equal to 2 or 8, T_{amb} was replaced by the building air temperature, T_{room}. Otherwise, the equations were still applicable.

Another term was added to the heat balance equation describing the collector air temperature. This term represented the heat transfer, due to the fan, from the collector air to the room air. It was of the form $\dot{m}c_p(T_{air} - T_{room})$. Since it represented a heat loss from the collector air, it was inserted with a negative sign. Applying this modification to Equation (2.8) resulted in

$$\sum_{i=1}^{11} A_i h_i (T_i - T_{air}) - r(mc)_{air}(T_{air} - T_{amb}) - \dot{m}c_p(T_{air} - T_{room}) = (mc)_{air} \frac{dT_{air}}{dt} . \quad (2.15)$$

The temperature of the building air, T_{room}, was the most important result desired from the isolated gain model. To determine this temperature, a differential equation describing it was needed. The equation was derived in the same manner as for the collector air temperature. A heat balance, equating net heat gains to storage, resulted in

$$\dot{m}c_p(T_{air} - T_{room}) - UA_{tot}(T_{room} - T_{amb}) + A_2(T_2 - T_{room})/R_2 + A_8(T_8 - T_{room})/R_8 = (mc)_{room} \frac{dT_{room}}{dt} . \quad (2.16)$$

The first term in this equation represents the heat provided to the building air from the collector air (due to the fan). The second term represents the heat loss to the ambient. UA_{tot} is the total building heating load, including infiltration. The other two terms on the left-hand side of the equation represent conduction, through the wall, from

the collector storage to the room air. The right-hand side of Equation (2.16) represents the storage. If this storage, and hence the time constant of the air, was neglected, the room air temperature fluctuated wildly and the results were unusable.

The differential equations for this model were solved by the same method as was used for the direct gain model. A first-order approximation was made for the time derivative in each differential equation, and the equations were solved for the new temperatures. This procedure had a truncation error on the order of Δt^2. The resultant expression for the new collector air temperature was found to be

$$T'_{air} = \frac{\Delta t}{(mc)_{air}} \left\{ \sum_{i=1}^{11} A_i h_i T_i + r(mc)_{air} T_{amb} + \dot{m}c_p T_{room} + \left[\frac{(mc)_{air}}{\Delta t} - r(mc)_{air} - \dot{m}c_p - \sum_{i=1}^{11} A_i h_i \right] T_{air} \right\}. \quad (2.17)$$

The resultant expression for the new room air temperature was

$$T'_{room} = \frac{\Delta t}{(mc)_{room}} \left\{ \dot{m}c_p T_{air} + UA_{tot} T_{amb} + A_2 T_2 / R_2 + A_8 T_8 / R_8 + \left[\frac{(mc)_{room}}{\Delta t} - \dot{m}c_p - UA_{tot} - A_2/R_2 - A_8/R_8 \right] T_{room} \right\}. \quad (2.18)$$

There were, or course, different limitations on Δt, which were determined from Equations (2.11) (with the previously discussed changes), (2.17), and (2.18). These limits were

$$\Delta t \leq \frac{(mc)_i/A_i}{(h_i + 1/R_i)}, \tag{2.18}$$

$$\Delta t \leq \frac{(mc)_{air}}{r(mc)_{air} + \dot{m}c_p + \sum_{i=1}^{11} A_i h_i}, \tag{2.19}$$

and

$$\Delta t \leq \frac{(mc)_{room}}{\dot{m}c_p + UA_{tot} + A_2/R_2 + A_8/R_8} \tag{2.20}$$

The computer model for the isolated gain system was virtually identical to the direct gain model, except for the modifications discussed in this section. The same restrictions on the data time step were applicable.

Trombe Wall Model

A Trombe wall passive solar system is one type of indirect gain system. It consists of a large window with a masonry wall for thermal storage located a short distance behind the window. Vents in the top and bottom of the wall allow room air to be heated by natural convection over the sun side of the wall. Back-draft dampers are necessary to prevent reverse circulation of the air at night. If reverse circulation is not prevented, the vents are, in the absence of night (collector) window insulation, a net thermal disadvantage to the system [3].

Figure 2.6 illustrates a Trombe Wall system and the modes of heat transfer used to develop this model. Sunlight is absorbed by the sun side surface of the wall. This heat is convected to the air space and conducted through the storage wall. Flow of air through the vents, convection from the room side surface of the storage wall and convection from the room's interior surfaces heat the room air. The room air was assumed to be transparent to thermal radiation from the storage wall, and only radiative interactions with the interior surfaces were considered.

A heat balance, equating net heat gains to storage, was used to derive the differential equation describing the thermal response of the room air. This equation was found to be

$$h_b A_{wall}(T_w(b,t) - T_{room}) + (UA)_{int}(T_{int} - T_{room}) + r(mc)_{room}(T_{amb} - T_{room}) + \dot{m}c_p(T_{out} - T_{room}) = (mc)_{room}\frac{dT_{room}}{dt} \quad (2.21)$$

The first term represents convection from the interior surface of the storage wall. The second term accounts for convection from the room's interior surfaces. The third term represents the heat loss to the ambient due to infiltration, and the fourth term represents heat gain by air flow through the vents. The right-hand side of the equation represents thermal storage in the room air.

In this model, thermal interactions between the interior surfaces of the room and the rest of the room were considered to be important.

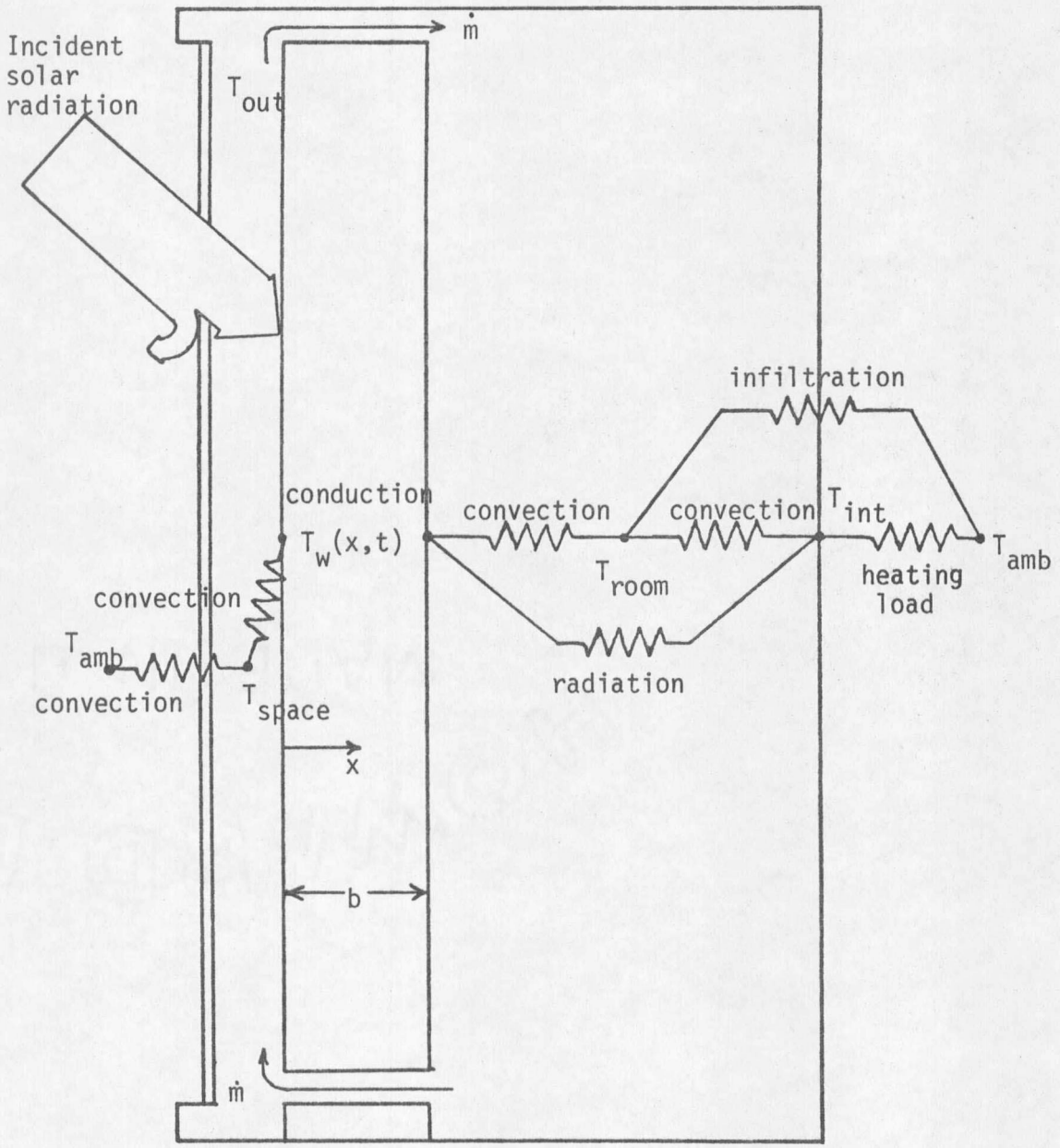


Figure 2.6 Trombe Wall System and Principal Modes of Heat Transfer

The entire inside surface of the room (excluding the storage wall) was treated as one isothermal, lumped-capacity body. The differential equation describing the thermal response of the room's interior surface was obtained using a heat balance similar to that used for the room air. The resultant equation was

$$Q_r + UA_{int}(T_{room} - T_{int}) + UA_{tot}(T_{amb} - T_{int}) = (mc)_{int} \frac{dT_{int}}{dt} \qquad (2.22)$$

where Q_r is the radiative heat transfer rate from the storage wall, given by

$$Q_r = \frac{A_{wall}\sigma(T_w^4(b,t) - T_{int}^4)}{\frac{1 - \varepsilon_{wall}}{\varepsilon_{wall}} + 1 + \frac{A_{wall}}{A_{int}} \frac{1 - \varepsilon_{int}}{\varepsilon_{int}}} . \qquad (2.23)$$

The second term in Equation (2.22) represents convection from the interior surface to the room air. The third term represents heat loss (by conduction through the walls) to the ambient. The right-hand side of the equation accounts for thermal storage in the room's interior surface. This storage was assumed to be significant.

In order to simulate the total thermal response of the system, the temperature distribution in the storage wall, as a function of time, was needed. The wall was approximated as a one-dimensional, transient heat flow problem. The general differential equation for this type of conduction problem is

$$\frac{\partial^2 T_w}{\partial x^2} = \frac{1}{\alpha} \frac{\partial T_w}{\partial t} . \tag{2.24}$$

The wall also had the initial condition

$$T_w(x,0) = f(x) \tag{2.25}$$

and the boundary conditions

$$-k \frac{\partial T_w}{\partial x}\bigg|_{x=0} = Q_s + h_0 A_{wall}[T_{space} - T_w(0,t)] \tag{2.26}$$

and

$$-k \frac{\partial T_w}{\partial x}\bigg|_{x=b} = Q_r + h_b A_{wall}[T_w(b,t) - T_{room}]. \tag{2.27}$$

The average air space temperature, T_{space}, was found by equating the heat delivered to the room (via the vents) to the sum of the convection from the storage wall to the air space and from the air space (through the window) to the ambient. This resulted in

$$T_{space} = \frac{2\dot{m}c_p T_{room} + A_{win}T_{amb}/R_{win} + h_0 A_{wall} T_w(0,t)}{2\dot{m}c_p + A_{win}/R_{win} + h_0 A_{wall}}. \tag{2.28}$$

The vent outlet temperature, T_{out}, was found using

$$T_{out} = 2T_{space} - T_{room}. \tag{2.29}$$

The mass flow rate of air through the vents, $\dot{m}$, was also needed. It was found using

$$\dot{m} = \rho_{air} A_{win} [C_d A'_v \sqrt{g\beta |T_{out} - T_{room}|/H}]. \qquad (2.30)$$

The term within the brackets was developed by Balcomb et al [3] and represents the volumetric flow rate per unit area of glazing. The air density, ρ_{air}, was calculated using the ideal gas law.

Equations (2.21) and (2.22) were solved using the same method as was used for the direct gain model. A first-order, finite difference approximation was made for each time derivative, and the equations were then solved for the new temperatures. This approximation resulted in a truncation error on the order of Δt^2. The explicit expression for the room's new interior surface temperature was found to be

$$T'_{int} = \frac{\Delta t}{(mc)_{int}} \left\{ Q_r + (UA)_{int} T_{room} + UA_{tot} T_{amb} + \left[\frac{(mc)_{int}}{\Delta t} - (UA)_{int} - UA_{tot} \right] T_{int} \right\} . \qquad (2.31)$$

The new room temperature was calculated using

$$T'_{room} = \frac{\Delta t}{(mc)_{room}} \left\{ h_b A_{wall} T_w(b,t) + (UA)_{int} T_{int} + r(mc)_{room} T_{amb} + \dot{m} c_p T_{out} + \left[\frac{(mc)_{room}}{\Delta t} - h_b A_{wall} - (UA)_{int} - r(mc)_{room} - \dot{m} c_p \right] T_{room} \right\} . \qquad (2.32)$$

The differential equation describing the storage wall temperature distribution (Equation (2.24)) was solved using a finite difference technique suggested by Carnahan et al [18]. The wall was divided into n lumped-capacity nodes, evenly spaced Δx apart, as shown in Figure 2.7. Nodes 1 and n were $\frac{\Delta x}{2}$ thick, and the other (interior) nodes were all Δx thick. A first-order approximation for the time derivative and a second-order approximation for the space derivative were substituted into Equation (2.24). The equation was then solved for the new temperature of each node, resulting in

$$T'_{wi} = \lambda T_{wi-1} + (1 - 2\lambda)T_{w_i} + \lambda T_{w_{i+1}} \tag{2.33}$$

where

$$\lambda = \frac{\Delta t \alpha}{\Delta x^2} . \tag{2.34}$$

These equations are only applicable to interior nodes ($2 \leq i \leq n-1$), and resulted in a truncation error on the order of $(\Delta x^3 + \Delta t^2)$.

Two methods were available to satisfy the boundary conditions of the storage wall (Equations (2.26) and (2.27)). The first of these was to linearly approximate $\frac{\partial T_w}{\partial x}$ and solve explicitly for the boundary temperatures. This method was not used because it ignored the thermal storage of the boundary nodes. This storage was only half that of each interior node, but was considered to be significant, especially for coarse grid spacings.

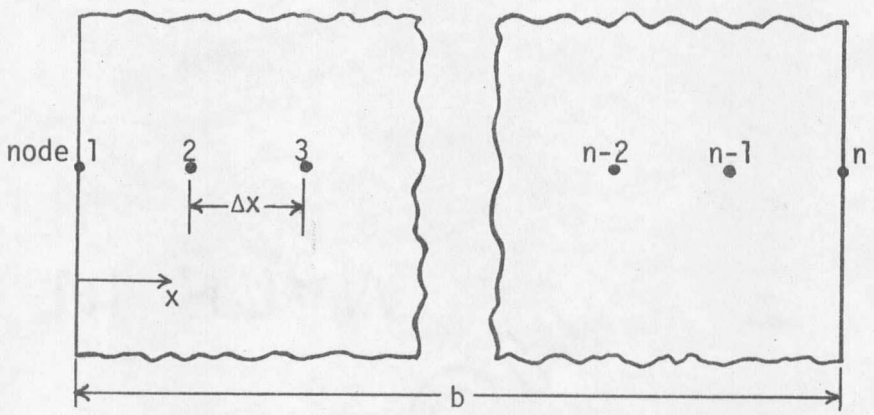


Figure 2.7 Node Configuration for the Storage Wall Solution

The method which was used involved performing a heat balance on each boundary node. The balance equated net thermal gains to storage. A first-order approximation for each time derivative was then substituted and the resultant equations were solved for the new boundary temperatures. The resulting equation for node 1 was

$$T'_{w1} = \frac{2\Delta t}{\rho c \Delta x}\left[Q_s/A_{wall} + h_0 T_{space} + \frac{k}{\Delta x} T_{w2} + \left(\frac{\rho c \Delta x}{2\Delta t} - h_0 - \frac{k}{\Delta x}\right) T_{w1}\right]. \quad (2.35)$$

The explicit equation for the new temperature of node n was found to be

$$T'_{w_n} = \frac{2\Delta t}{\rho c \Delta x}\left[-Q_r/A_{wall} + h_b T_{room} + \frac{k}{\Delta x} T_{w_{n-1}} + \left(\frac{\rho c \Delta x}{2\Delta t} - h_b - \frac{k}{\Delta x}\right) T_{w_n}\right]. \quad (2.36)$$

In order to guarantee stability of the numerical method, limits on Δt were needed. They were derived from the explicit Equations (2.31) through (2.36), using the non-negative condition cited earlier. The limitations on Δt were thus found to be

$$\Delta t \leq \frac{(mc)_{int}}{(UA)_{int} + UA_{tot}} , \tag{2.37}$$

$$\Delta t \leq \frac{(mc)_{room}}{h_b A_{wall} + (UA)_{int} + r(mc)_{room} + \dot{m}c_p} , \tag{2.38}$$

$$\Delta t \leq \frac{\Delta x^2}{2\alpha} , \tag{2.39}$$

$$\Delta t \leq \frac{\rho c \Delta x}{2(h_0 + k/\Delta x)} , \tag{2.40}$$

and

$$\Delta t \leq \frac{\rho c \Delta x}{2(h_b + k/\Delta x)} . \tag{2.41}$$

Equations (2.23) and (2.28) - (2.41) were used to write a computer code to simulate the thermal response of an indirect gain passive solar system of the Trombe wall type. The model is also applicable to solid wall systems (systems with no vents) merely by setting A_v' equal to zero. The model used essentially the same programming logic as did the direct gain model (see Figure 2.4). The only differences in the logic were the elimination of the geometry solution and of the complex radiation solution. Since the radiative heat transfer for the Trombe wall system is

given explicitly by Equation (2.23), it was recalculated each time the new system temperatures were calculated. The new storage wall temperature distribution was calculated first, then the new air temperature. The new interior surface temperature was calculated last. All of these calculations were based on the old system temperatures. The new air space and vent outlet temperatures were then calculated, using the other new temperatures. This procedure was followed for each successive time step.

The direct gain model has tight restrictions on the allowable interval between successive data sets (data time step). This is due to holding the radiative heat transfer rates constant for several successive time steps. This model, however, does not have the same restrictions, because the radiative heat transfer is recalculated for each time step. During the model validation procedure, the allowable data time step for this model was found to be one hour.

Model Validation

The direct gain and Trombe wall models were verified using data from passive test cells at the National Center for Appropriate Technology (NCAT), located in Butte, Montana. Data for isolated gain and natural passive systems were not available. However, since their models are essentially the same as the direct gain model, they may be as accurate as the direct gain model.

The direct gain model was validated for an eight day period beginning November 14 and ending November 21, 1978. Figure 2.8 illustrates the measured and simulated test cell air temperatures. Also shown are the ambient temperature and the insolation. The test cell air temperature was measured using a shielded thermocouple [19] located near the center of the test cell. The insolation was the total incident solar radiation (for the preceding hour) measured on a vertical, south-facing surface. The data were obtained from a report by Bickle/CM [20], which was submitted to the Solar Energy Research Institute (SERI) on June 12, 1979. The report contained hourly NCAT insolation and ambient temperature data for fourteen days. Hourly globe temperatures for a direct gain and Trombe wall test cell were also included in the report. The globe temperature was an approximation of the mean radiant temperature of each system. It was measured with a thermocouple inside a toilet bowl float (sphere). The float was painted black and was suspended in the center of the test cell approximately 30.5 cm (1 foot) from the ceiling. The direct gain test cell air temperatures were obtained from Larry Palmiter at NCAT. The globe temperature data were not used for the direct gain model validation. Instead, the air temperature was used, because of the difficulty of calculating the globe temperature. The difficulty arose because of the presence of diffuse sunlight at every point in the test cell. The diffuse sunlight caused the measured globe temperatures to be higher than the temperatures of the surfaces in

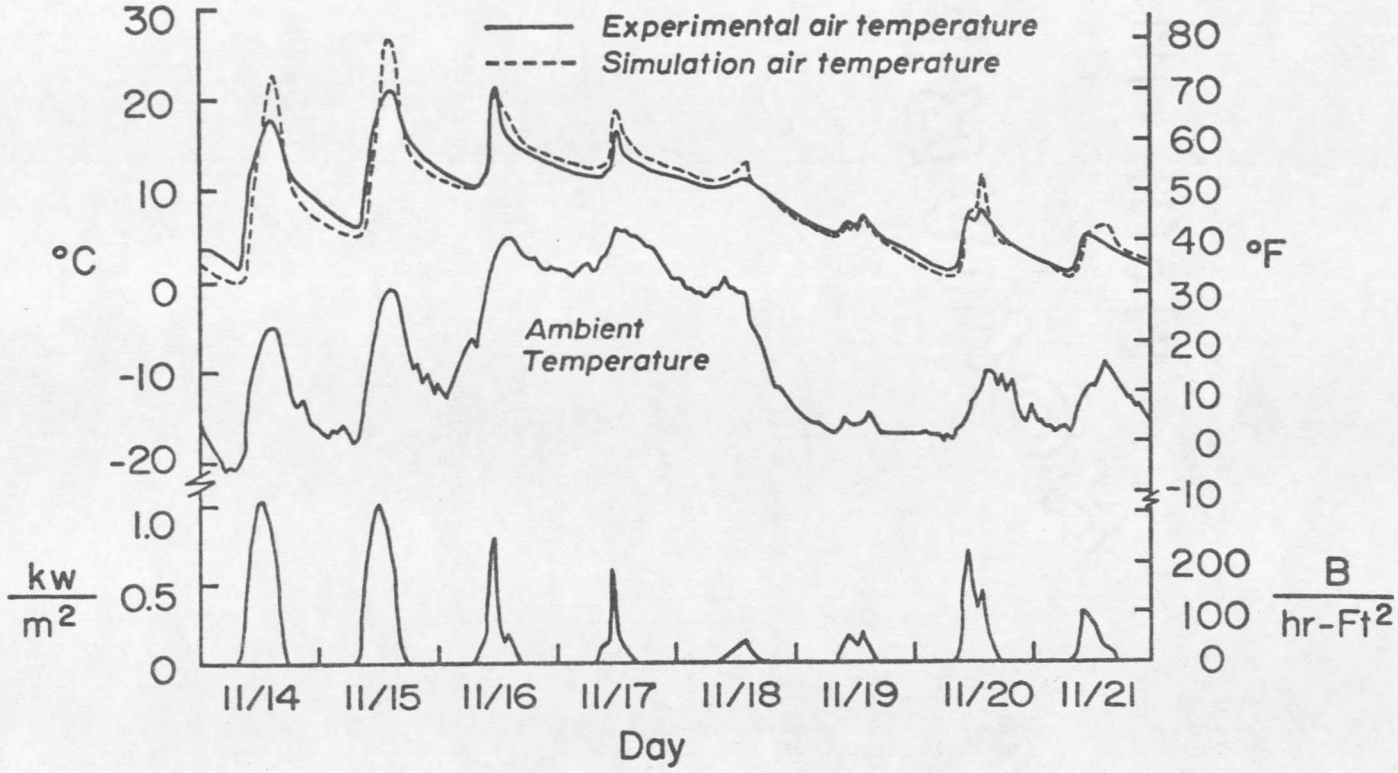


Figure 2.8 Direct Gain Validation

the room.

Inspection of Figure 2.8 shows good agreement between the measured and simulated air temperatures. The mean deviation of the simulated temperature from the measured values was 0.1°C (0.2°F) for the eight-day period. The root mean square (rms) deviation was 1.4°C (2.6°F) and the maximum deviation was 5.4°C (9.7°F).

The Trombe wall system model performance was verified for a six-day period beginning November 19, 1978. The simulated globe temperature was estimated using a mathematical approximation of a sphere with the same size and location as the measuring device in the test cells. A sphere 10.1 cm (4 inches) in diameter with an emissivity of 0.95 was located in the center of the room, 30.5 cm (1 foot) from the ceiling. Radiative interactions between the sphere and the storage wall and between the sphere and the room's interior surface were considered. Convection from the sphere to the air was also considered. A steady heat balance on the sphere was used to approximate its temperature. Figure 2.9 shows the measured and simulated globe temperatures for the test cell. The ambient temperature and insolation are also included. The simulated temperature shows good agreement with the measured values. During the first two days, the deviation of the simulation results from the data is relatively large. This is due to inaccuracies in the initial temperatures which were used for the simulation. However, the model exhibits the ability to overcome these initial inaccuracies and becomes more accurate as the

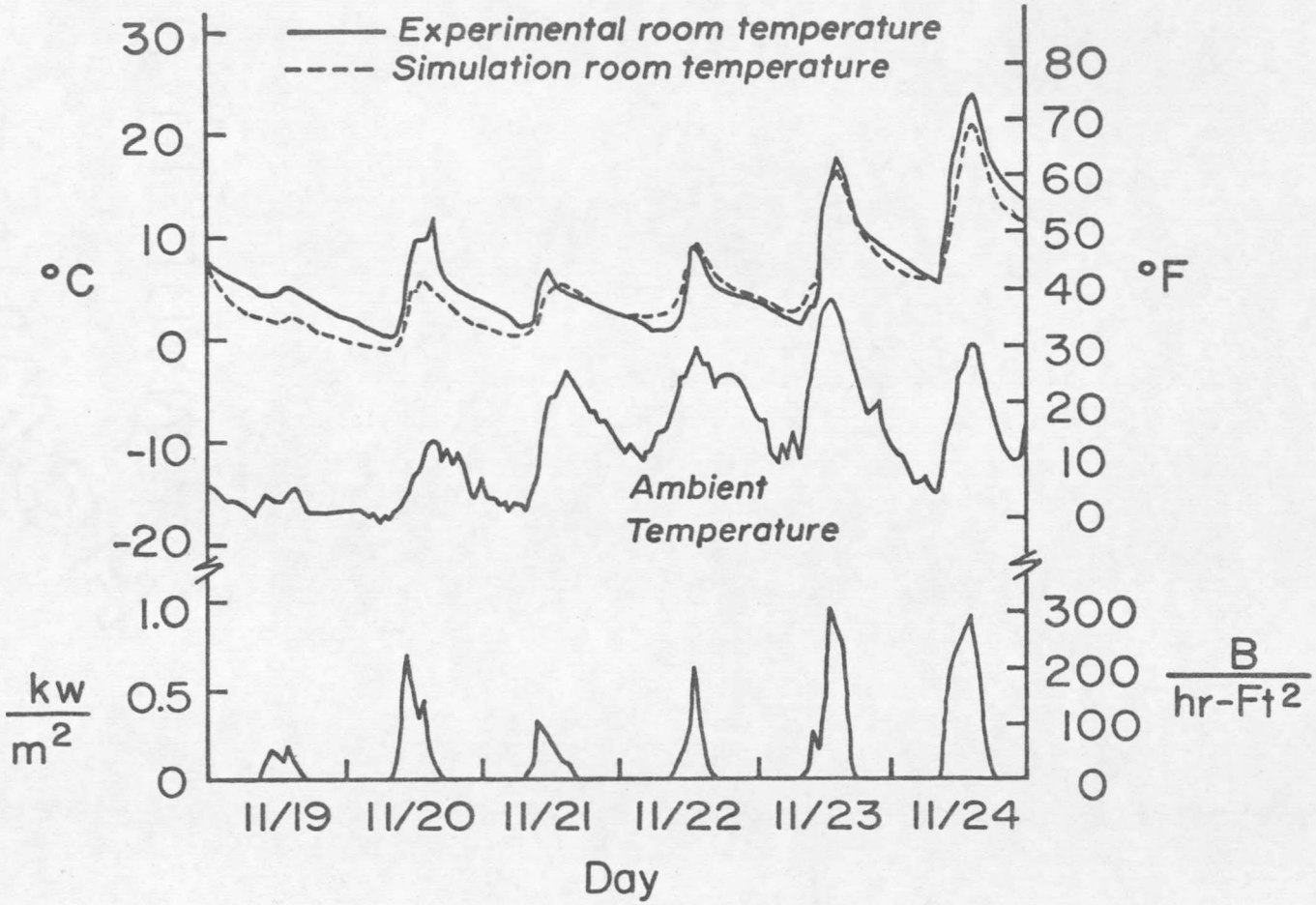


Figure 2.9 Trombe Wall Validation

the simulation proceeds. This is a good property for a model to possess because the model is thus self-correcting. The mean deviation of the simulated temperature from the measured was -1.1°C (-1.9°F) for the period. The rms deviation was 2.0°C (3.6°F) and the maximum deviation was 7.2°C (13°F).

CHAPTER III

RESULTS

The purpose of this study was to perform a comparison of four basic types of passive solar heating systems. The types compared were direct gain, indirect gain, isolated gain and natural passive systems. A computer model was developed to simulate the thermal response of each type of passive system, as described in Chapter II. A Trombe wall system was chosen to represent the indirect gain systems, since it is the most common type of passive solar system in use today. Natural passive systems were included because it was suspected that relocation of the normal window area present in a house to the south side of the building would result in significant solar heating. A direct gain (or natural passive) system is illustrated in Figure 2.1. A Trombe wall and an isolated gain system are shown in Figures 2.6 and 2.5, respectively.

The four passive systems were simulated for two six-day periods of different clear and cloudy day groupings. Total insolation and the ambient temperature variation were identical for the two periods. The first period, case I, consisted of three clear days followed by three cloudy days. This represented a "worst" case situation, where the thermal storage of each system was required to heat its building for a relatively long, low-insolation period. The second grouping, case II, began with a clear day which was followed by alternating cloudy and clear days. This represented a "best" case situation where the storage of each system was allowed one full clear day to recharge before being called upon

to heat its building for the next (cloudy) day. For reasons explained in Chapter II, hourly and sub-hourly insolation and ambient temperature data were required in order to perform the desired simulations. Since actual measured data of the desired form were not available for Bozeman, Montana, the required data were generated such that they represented typical mid-winter conditions in Bozeman. The ambient temperature data had 8.55°C days (heating) and 18.3°C nights each day. The total daily insolation was required to be 3.76 kw-hr/m^2 glazing (1195 Btu/ft^2) for clear days and 10% of this on cloudy days. The cloudy day insolation was determined from experimental data. Study of insolation data from Butte, Montana and Los Alamos, New Mexico revealed that the total insolation on cloudy days is approximately 10-12% of that of clear days. Appendix E contains the equations (and their derivations) which were used to generate the necessary data from these average conditions.

Each passive solar system was incorporated into a well-insulated single floor dwelling with a floor area of 139 m^2 (1500 ft^2). The house was constructed such that the equivalent R-factors of the building components were:

Foundation Perimeter	$R = 0.88 \frac{m^2\ °C}{w}$, $(5 \frac{hr\text{-}ft^2\text{-}°F}{Btu})$;
Walls	R = 3.35, (19);
Ceiling	R = 6.69, (38); and
Windows	R = 0.359, (2.04).

All windows (including the collector) were assumed to be covered with R 1.76 $\frac{m^2°C}{w}$ (10 $\frac{hr\text{-}ft^2\text{-}°F}{Btu}$) insulation at night because of the increase in thermal efficiency which passive solar heating systems always exhibit with its use [10,11]. The infiltration rate was taken to be 1/2 air change per hour. The collector area, thermal storage and heating load were identical for the formal passive (direct, indirect, and isolated gain) systems. This was done so that the systems would be compared under identical conditions. The thermal storage of the direct gain system was assumed to be distributed evenly over the portion of the room receiving direct insolation (i.e. the floor, north, west, and east walls). The thermal storage of the indirect gain system was concentrated in a high density (2400 kg/m^3) concrete wall 40.6 cm (16 in.) thick, located 30.5 cm (1 ft) from the window. The isolated gain system was assumed to be a direct gain system 3.05 m (10 ft) deep by 15.2 m (50 ft) long attached to the south wall of the house. The thermal storage was distributed evenly over the collector's floor and north wall, because those two surfaces received most of the insolation. A fan which delivered approximately 0.236 m^3/s (500 cfm) of air was used to provide air interchange between the collector and the house.

The natural passive system was simulated for two different window areas. The first area was approximately the normal window area present in a house. All windows were assumed to be located on the south wall of the building, so all could provide solar heating. The second window

area was approximately one half of that used in the formal passive systems. The thermal storage of the natural passive systems was estimated by summing the thermal storage of all internal walls. They were constructed of 2" x 4" wooden studs with 1/2" gypsum board on both sides. In addition, the inside surfaces of the external walls (1/2" gypsum board) were assumed to store heat. The thermal storage of the building's contents was approximated as equal to that of the house itself. This estimate is probably conservative, since most houses contain several large, massive appliances, such as a refrigerator and a stove, in addition to cabinets, furniture, and other property. The storage was then distributed evenly over the floor, north, west, and east walls. The collector window area and thermal storage of each simulated system are listed in Table 3.1.

The temperatures of the passive system components were initialized such that the thermal storage of each was nearly fully charged before the first cloudy day was encountered. All components of the direct gain, isolated gain and natural passive systems were initialized at 18.3°C (65 °F), since the time constant of their storage is short (one day or less). The indirect gain system's storage wall temperature distribution was initialized somewhat higher because its time constant is larger (several days). These initial conditions were combined with the physical parameters and weather data cited above and used to simulate the passive systems (except the isolated gain system) with no auxiliary heating.

Table 3.1 Physical Parameters of the Passive Solar Systems

System Type	Window (Collector) Area m^2 (ft^2)	Thermal Storage kw-hr/°C (Btu/°F)
Direct Gain	34.8 (375)	6.85 (13000)
Indirect Gain (Trombe Wall)	34.8 (375)	6.85 (13000)
Isolated Gain	34.8 (375)	6.85 (13000)
Natural Passive	9.26 (100)	2.74 (5200)
	17.7 (190)	2.74 (5200)

The room air temperature of each system was allowed to "float" with no upper or lower limits. The systems were then simulated with auxiliary heating. Whenever the air temperature was calculated as being less than 15.6°C (60°F), it was reset to 15.6°C. A term, equal to the auxiliary heat supplied, was then added to the air energy balance equation to maintain the balance. The total auxiliary heat supplied for the test period was printed at the end of each simulation. The isolated gain system was simulated only with auxiliary heating. If the collector air temperature was higher than the building air temperature, the fan controlling air flow between the collector and the building was turned on whenever the

building air temperature dropped below 15.6°C. It was turned off if the building air temperature rose above 21.1°C (70°F), or if the collector air temperature was less that the building air temperature. The auxiliary heating was calculated in the same manner as it was for the other three systems.

The results of the direct and indirect gain simulations, without auxiliary heating, are illustrated, for cases I and II, in Figures 3.1 and 3.2, respectively. Also shown are the ambient temperature and insolation distributions for both cases. The direct gain system, as expected, exhibits larger air temperature fluctuations for both cases. The indirect gain system maintains a higher air temperature during the cloudy days of both cases. For case II, both systems experience a higher final air temperature (at the end of day 6). This is due to the lower peak and mean air temperatures which occur, on clear days, in case II. Lower temperatures result in lower heat loss rates, which in turn cause the storage to lose less heat over the period, resulting in higher final temperatures. Figures 3.3 and 3.4 illustrate the results of the natural passive systems (for both window areas) for cases I and II, respectively. Both systems exhibit large air temperature fluctuations. For both cases, the fluctuations are larger than those of the direct gain system. This is due to the relatively small thermal storage of the natural passive systems (see Table 3.1). These systems also experience higher final air temperatures for case I than for case II. However, the difference in

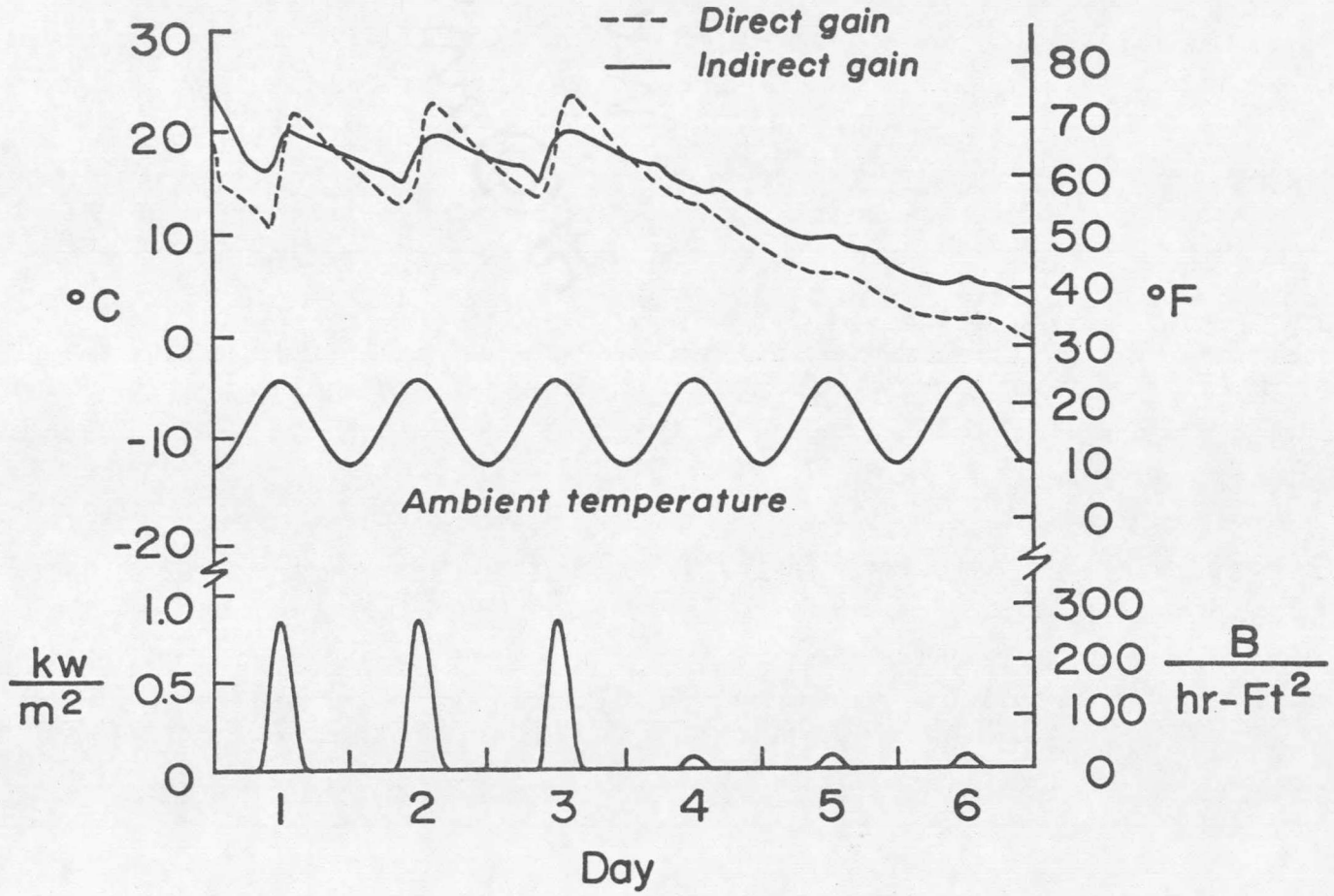


Figure 3.1 Direct-Indirect Gain Comparison Without Auxiliary Heating, Case I.

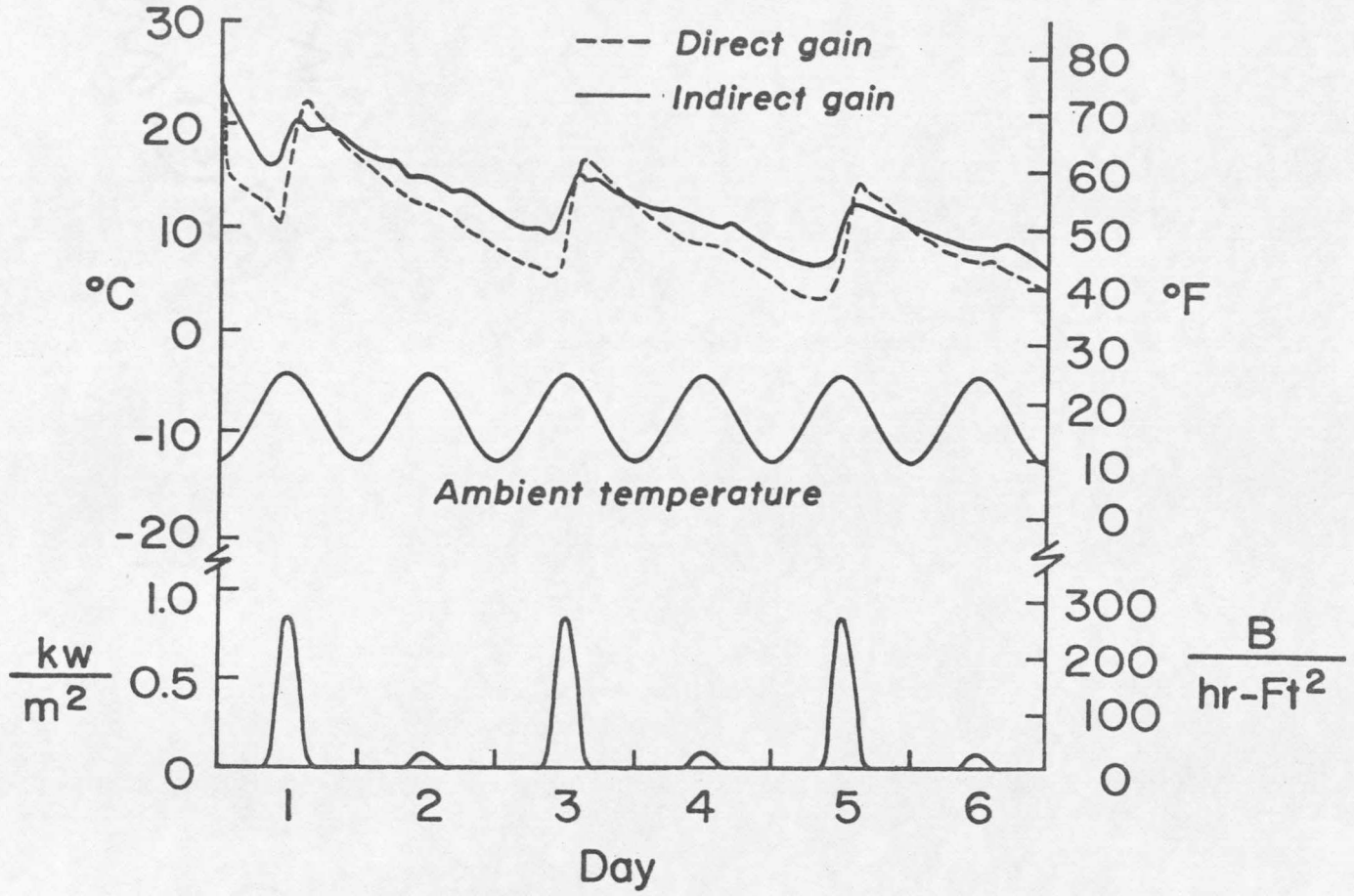


Figure 3.2 Direct-Indirect Gain Comparison Without Auxiliary Heating, Case II.

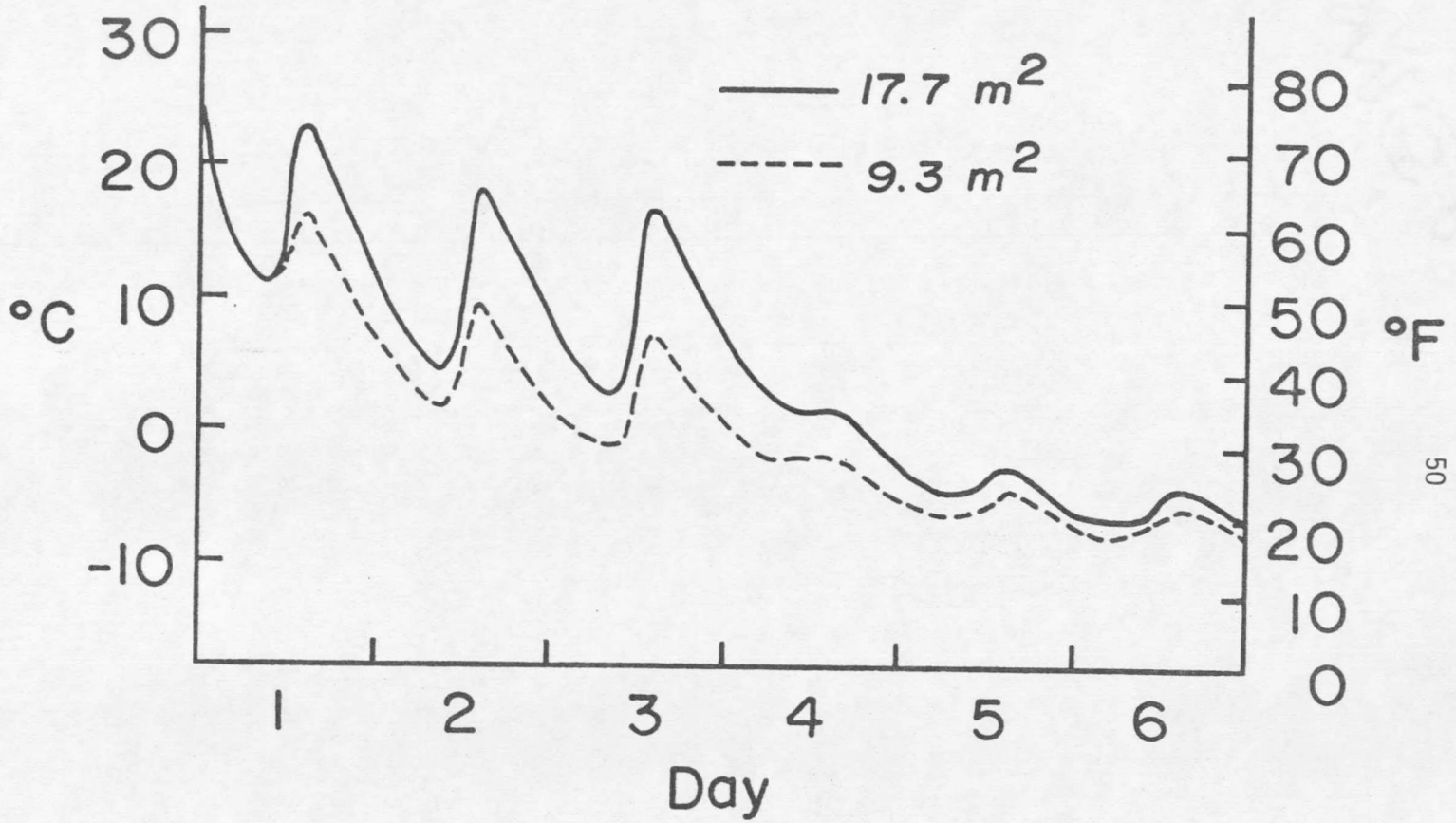


Figure 3.3 Natural Passive Air Temperature Without Auxiliary Heating, Case I.

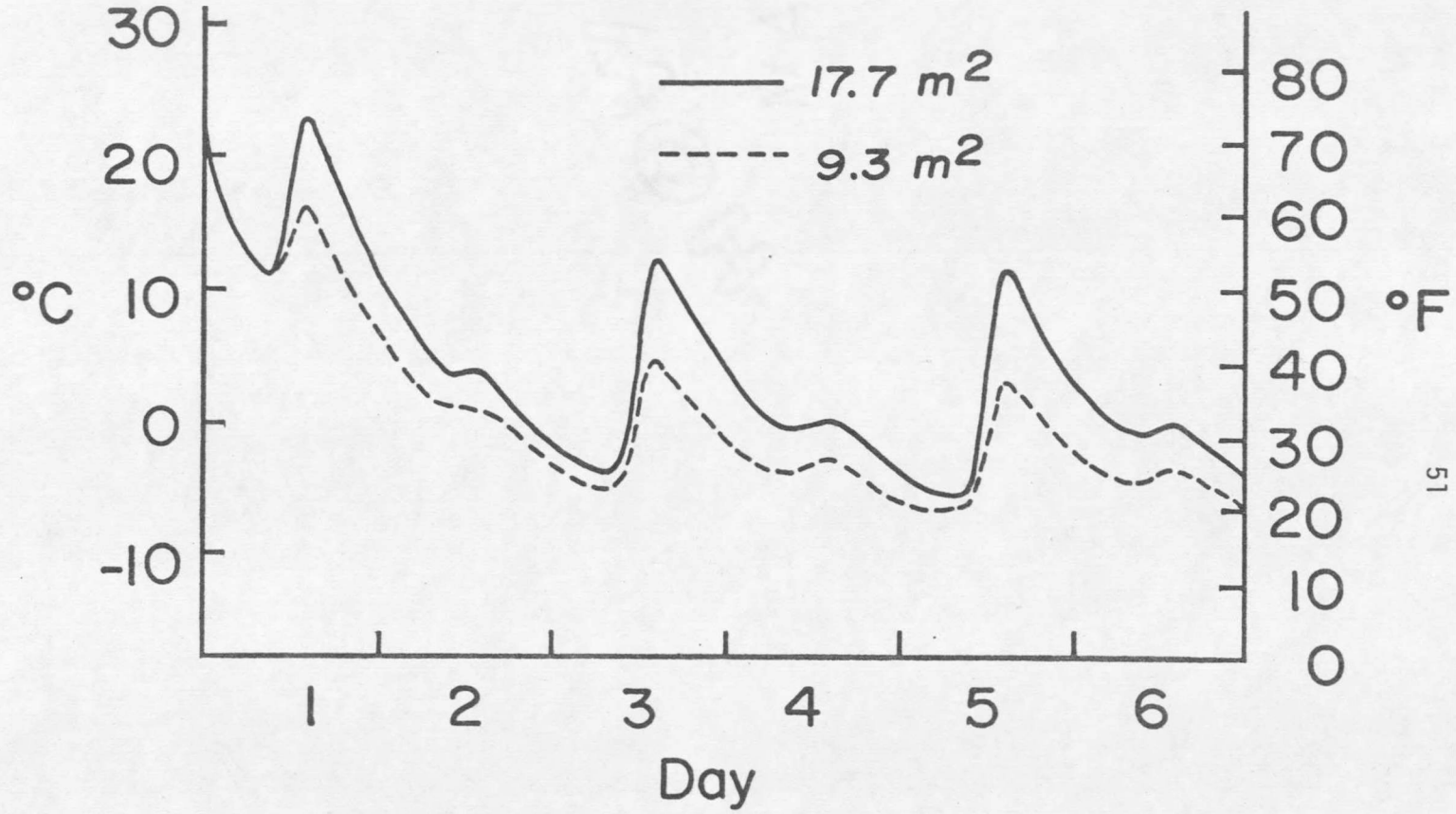


Figure 3.4 Natural Passive Air Temperature Without Auxiliary Heating, Case II.

final temperatures (between the two cases) is less than that for either the direct or indirect gain systems. Naturally, the air temperature is greater for the larger window area system in both cases. The air temperature of the three systems (direct gain, indirect gain, and natural passive) is maintained well above ambient by the solar heating. None of the systems performs well on cloudy days, showing little or no air temperature increase due to absorption of cloudy day insolation, since losses to the ambient outweigh these gains.

The results of the simulations of the direct and indirect gain passive solar heating systems, with auxiliary heating, are illustrated in Figures 3.5 and 3.6. Both systems maintain the air temperature at or above 15.6°C for the first three (clear) days of case I. The direct gain system required a small amount of nighttime auxiliary heating for the first three days because of its larger air temperature fluctuations. The indirect gain system maintains the air temperature above 15.6°C for the three days without the aid of auxiliary heating. The presence of auxiliary heating is evidenced by a uniform 15.6°C air temperature. Both systems drop to a steady air temperature of 15.6°C at about the same time early in the fourth day. Beyond this time, the air temperature is maintained by auxiliary heating. In case II (Figure 3.6), however, the direct gain system appears to outperform the indirect gain system. Both systems maintain the air temperature above 15.6°C for the first day, but both drop to and remain at 15.6°C for most of the second. During each

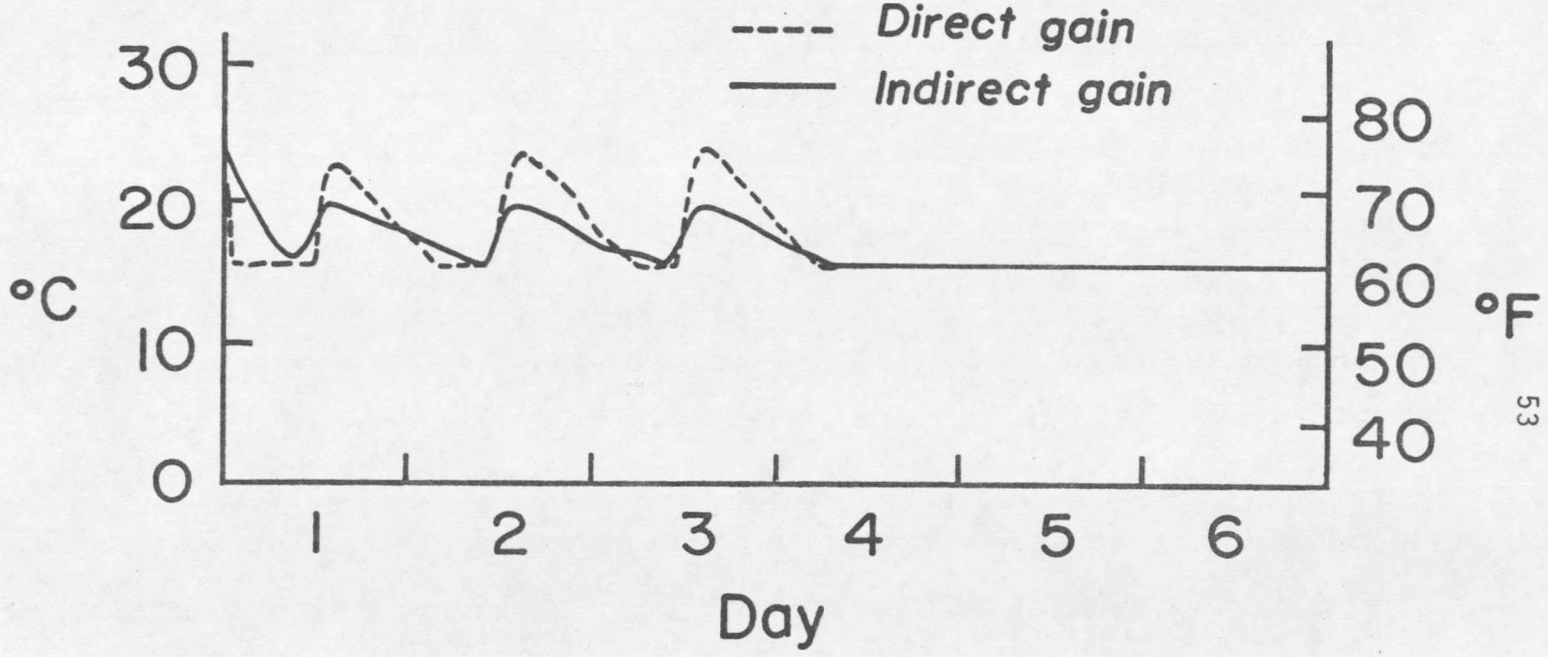


Figure 3.5 Direct-Indirect Gain Comparison with Auxiliary Heating, Case I.

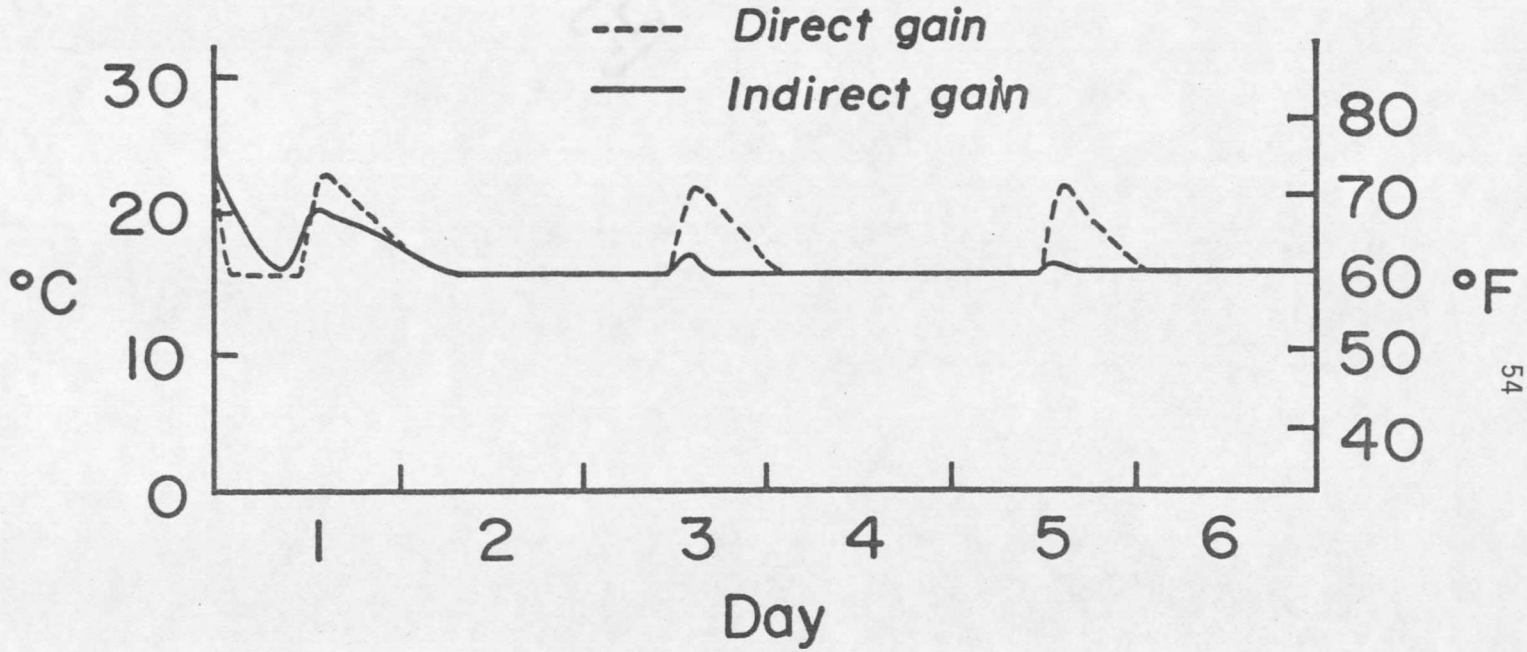


Figure 3.6 Direct-Indirect Gain Comparison with Auxiliary Heating, Case II.

succeeding clear day, the direct gain system attains about the same peak temperature, and the system supplies all the required heating for about 1/2 of each clear day. The indirect gain system, on the other hand, provides all the required heating only for shorter periods each succeeding clear day. The difference in the performance of the two systems is due to the difference in storage surface area. The direct gain system has a much larger storage surface area, which enables it to respond quickly to absorbed insolation.

Figures 3.7 and 3.8 illustrate the results of the test case simulations of the natural passive systems with auxiliary heating. The systems perform in much the same manner as the direct gain system. Both systems exhibit air temperatures in excess of 15.6°C during the sunny portion of each clear day, indicating that solar gain is providing all the necessary heat for that portion of the day. In both cases I and II, the height and length of the temperature peaks are (for each system) identical for each clear day after day 1. This is because the storage of each system has a relatively short time constant and thus reacts rapidly to absorption of solar radiation.

Figures 3.9 and 3.10 illustrate the hourly average building air temperature of the isolated gain system for cases I and II, respectively. Due to the action of the fan, which was turned on and off several times per hour, the building air temperature varied continuously between 15.6°C and 21.1°C. The fluctuation was greatest when the collector air

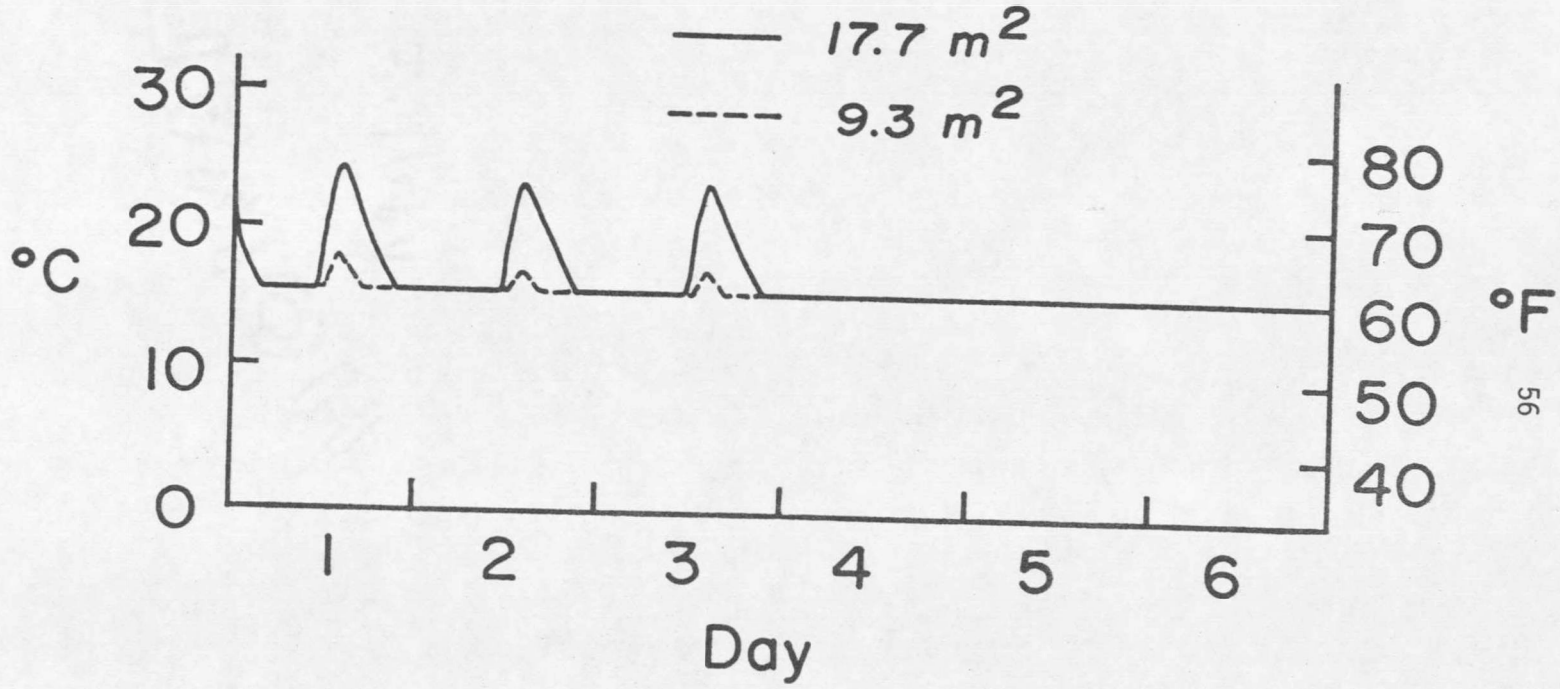


Figure 3.7 Natural Passive Air Temperature with Auxiliary Heating, Case I.

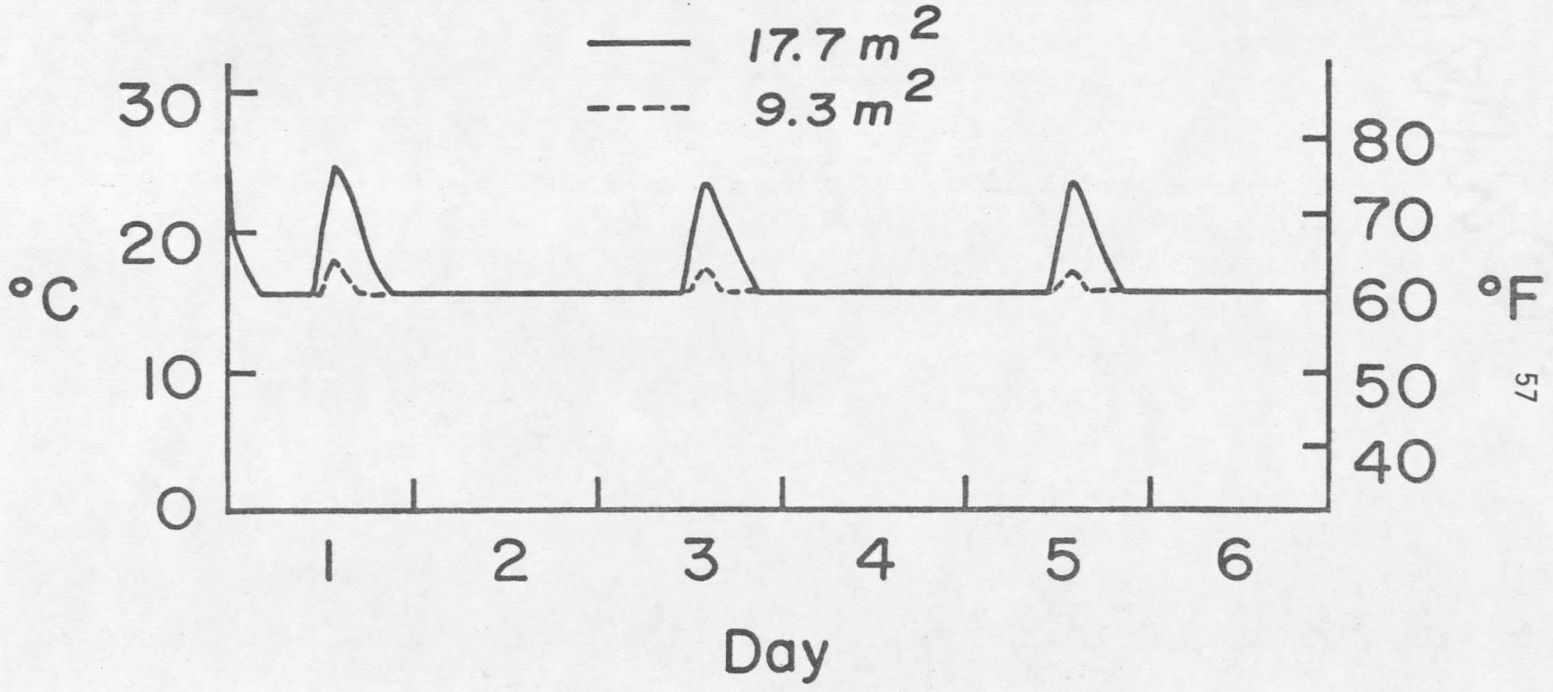


Figure 3.8 Natural Passive Air Temperature with Auxiliary Heating, Case II.

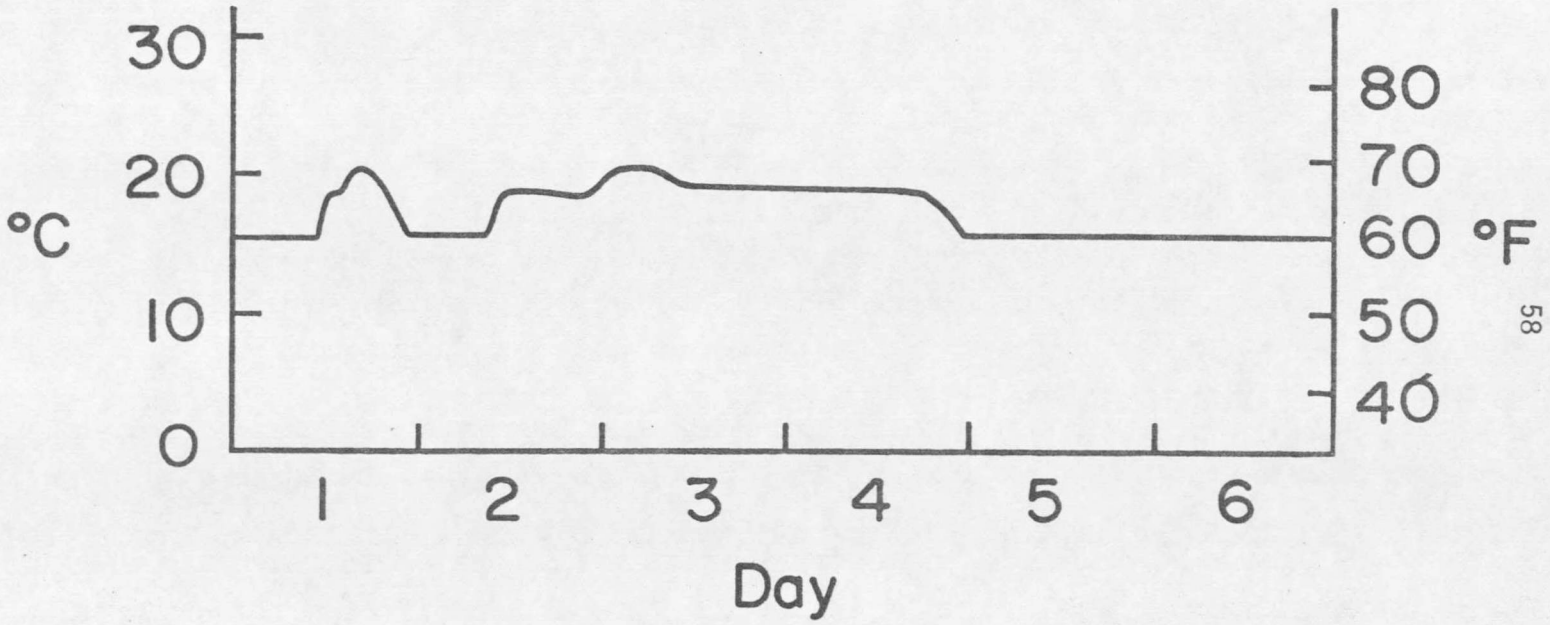


Figure 3.9 Isolated Gain Building Air Temperature with Auxiliary Heating, Case I.

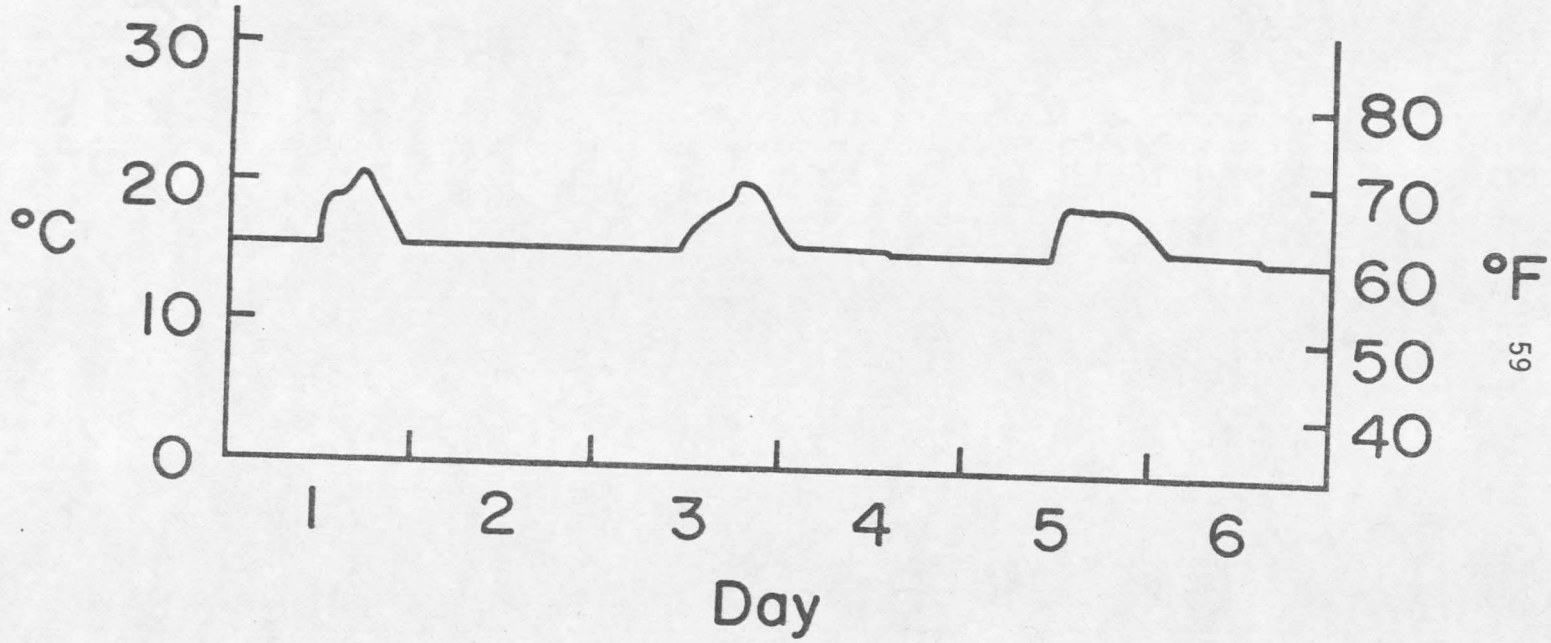


Figure 3.10 Isolated Gain Building Air Temperature with Auxiliary Heating, Case II.

temperature was much greater than the minimum temperature needed to heat the building. Whenever the collector air temperature fell to a level which allowed the fan to run continuously, an abrupt rise in the average building air temperature occurred. This situation caused the unexpected rise in building air temperature early in day 3 of case I. This phenomenon also caused the odd shapes of the temperature rises on day 1 of case I and on days 1 and 3 of case II. The isolated gain system demonstrates good solar heating capabilities by maintaining the building air temperature above 15.6°C, without the aid of auxiliary heating, well into the cloudy days of both cases.

In order to compare the performances of the simulated passive solar heating systems, some definition of system effectiveness is necessary. The most common measure of system effectiveness is the solar fraction. It is defined as the fraction of the building's heating load which is supplied by solar heating. The heating load was calculated for each system, using standard ASHRAE techniques [17], as the energy needed to maintain the building air temperature (above ambient) at 15.6°C (60°F) for the six-day period, without solar heating. During the simulations, the building air was heated only by heat from the thermal storage, the auxiliary heat source and solar radiation. The heat supplied by solar radiation was thus defined as

[solar heating] = [heating load] + [net change in thermal storage] - [auxiliary heating].

The net change in thermal storage was calculated from the initial and final storage temperatures. If the final storage temperature for a system was less than the initial temperature, the net change in thermal storage was negative. The solar fraction was then defined as the solar heating divided by the heating load. Table 3.2 lists the heating load, total auxiliary heat supplied, net change in thermal storage and the solar fraction of each simulated system, for both test cases.

As expected, the formal passive solar systems achieved higher solar fractions for the "best" case (case II) than for case I. However, the difference between the two cases is much smaller than was anticipated (only a few percent). This was probably due to the initial system temperatures and/or the length of the test periods. Inspection of Table 3.2 reveals that each system exhibits a different magnitude of performance change between the two test cases. Each natural passive system performs virtually the same for cases I and II. The isolated gain system, however, exhibits the largest difference in performance, while the direct and indirect gain system performances differ some, but not as much as those of the isolated gain system. The magnitudes of the differences seem to be directly related to the level of heat delivery control present in the system. The natural passive system with the larger collector window area produced a significantly larger solar fraction than did the one with the smaller window area. This result was expected, but inspection of the results for these two systems indicates that

Table 3.2 Auxiliary Heating and Solar Fractions for the Test Case Simulations

System	Heating Load kw-hr (10^6Btu)	Case I Auxiliary Heating kw-hr (10^5Btu)	Case I Net Change in Storage kw-hr (10^5Btu)	Case I Solar Fraction %	Case II Auxiliary Heating kw-hr (10^5Btu)	Case II Net Change in Storage kw-hr (10^5Btu)	Case II Solar Fraction %
Direct Gain	562 (1.92)	171 (5.85)	-19 (-0.65)	66.1	166 (5.68)	-19 (-0.65)	67.0
Indirect Gain	562 (1.92)	96 (3.27)	-112 (-3.82)	63.1	114 (3.90)	-82 (-2.81)	65.1
Isolated Gain	565 (1.93)	166 (5.68)	-19 (-0.65)	67.2	168 (5.75)	+19 (+0.65)	73.6
Natural Passive							
9.3m^2	486 (1.66)	316 (10.8)	-23 (-0.78)	30.2	316 (10.8)	-23 (-0.78)	30.2
17.7m^2	512 (1.75)	269 (9.19)	-23 (-0.78)	43.0	269 (9.18)	-23 (-0.78)	43.1

doubling the collector area does not double the solar fraction. This is in part due to the increase in heat loss which always accompanies increased window area.

For both test cases, the direct gain system outperformed the indirect gain (Trombe wall) system. This is consistent with the results of Wray and Balcomb [12] for storage mass to window area ratios in excess of 830 kg/m^2 (170 lb/ft^2). The ratio for the formal passive solar heating systems used in this study was 976 kg/m^2 (200 lb/ft^2).

CHAPTER IV

CONCLUSIONS

The results of this study indicate that passive solar heating systems are good means of space heating. With adequate collector area and thermal storage a passive system may heat a home for a fairly long cloudy period (one full day or longer); however, some source of make-up heat is often needed to maintain human comfort levels during these cloudy periods, especially in cold climates. For the conditions of this study, the direct gain system is a better choice for space heating than is the Trombe wall system. However, this does not mean that a direct gain system is a better choice than an indirect gain system, since water wall systems consistently out-perform Trombe wall systems [10], and may perform better than direct gain systems. Isolated gain systems, which are retrofittable, exhibit the potential to provide space heating comparable to direct and indirect gain systems with the same collector area and thermal storage.

Although formal passive solar heating systems may easily provide more than 50% of the space heating requirements of a dwelling under average mid-winter conditions in Bozeman, Montana, mere relocation of the normal window area present in a house onto the south wall of the building results in substantial solar heating. This relocation would be difficult and expensive for houses which have already been built, but would cost little or nothing at the original construction level. Night collector window insulation is desirable for use with all types of

passive solar heating systems because of the increase in thermal efficiency which always accompanies its use.

The performance of all passive solar systems seems to be dependent on the distribution of the incident solar radiation (insolation) over the period in question. The performance of passive systems appears to be best when the insolation is spread evenly over the period, such as when clear and cloudy days alternate. A decrease from this performance is exhibited by passive solar systems when the insolation is more concentrated, such as when clear and cloudy days occur in groups of three each. The magnitude of this decrease is dependent on the type of system considered. Natural passive systems, which exhibit large air temperature fluctuations when auxiliary heat is not supplied, experience a negligible decrease in performance from one distribution to the other. On the other hand, isolated gain systems, which control heat delivery to the building air better than the other types of passive systems studied, exhibit the greatest decrease in performance when clear and cloudy days occur in groups of three, rather than alternating. This seems to show a direct relationship between the degree of heat delivery control inherent in the system and the magnitude of the decrease in system performance (from one insolation distribution to the other). This trend is also exhibited by direct and indirect gain systems, and only applies to systems with equal collector area and thermal storage.

APPENDICES

APPENDIX A

SELECTION CRITERIA FOR LOCATION OF PROJECTED POINTS

Development of the direct gain model required a set of selection criteria to determine the location of projected window corner points. Table 2.1 lists the equations which were used to determine the coordinates of each projected point. However, these coordinate equations are dependent on where within the room the projected point falls. The equations are different for each surface (floor, north wall, west wall, and east wall) upon which the point may fall. The procedure which was used to determine the proper set of equations to use was as follows:

First, the point was checked to see if it fell on the floor. If this was true, then the insolation direction met

$$C_b \cot\gamma \leq W, \tag{A.1}$$

$$C_b - W\tan\gamma \leq 0, \tag{A.2}$$

and one of either

$$C_b + C_a \tan\gamma\cot\alpha \leq 0 \tag{A.3}$$

or

$$C_a - (L - C_a)\tan\gamma\cot\alpha \leq 0. \tag{A.4}$$

If these criteria were not met, then the north wall was checked. If the point fell on the north wall, the following conditions were met:

$$C_b \cot\gamma \geq W \tag{A.5}$$

and one of either

$$(L - C_a)\cot\alpha \geq W \tag{A.6}$$

or

$$-C_a\cot\alpha \geq W. \tag{A.7}$$

If these criteria were also not met, the west wall was tested. The point fell on the west wall if the insolation direction safisfied

$$-C_a\cot\alpha \leq 0, \tag{A.8}$$

$$C_a + C_b\cot\gamma\tan\alpha > L, \tag{A.9}$$

$$C_b - (L - C_a)\tan\gamma\cot\alpha \geq 0, \tag{A.10}$$

and

$$(L - C_a)\cot\alpha \leq W. \tag{A.11}$$

If none of the preceding sets of criteria were met, then the projected point fell on the east wall. However, in order to detect any errors in this method, the east wall was also tested. If the point was found not to fall on any of the four allowable surfaces, an error message was printed. This error message remained in the model throughout its development and use and was never encountered during any run. The projected point fell on the east wall if the following conditions were met:

$$(L - C_a)\cot\alpha \leq 0, \tag{A.12}$$

$$C_b + C_a \tan\gamma \cot\alpha \geq 0, \tag{A.13}$$

and

$$-C_a \cot\alpha \leq W. \tag{A.14}$$

These criteria were derived using physical reasoning combined with the inherent physical limitations of the direct gain system.

APPENDIX B

DETERMINATION OF THE SUNLIT AREA CONFIGURATION

The direct gain model contains a subroutine which generates equivalent rectangles for each sunlit area in the room (see Chapter II). There are 19 possible configurations that the sunlit areas could assume. Table B.1 lists the locations of the projected window corner points (A_p, B_p, C_p, and D_p) for each possible configuration. Each of these cases has its own set of equations for the calculation of the sizes and locations of the equivalent rectangles. Each of the sets was incorporated into the subroutine as an individual section, necessitating some means of determining which section to execute for any insolation direction. The programming logic which was used to accomplish the selection proceeded as follows:

A variable was used to indicate on which surface (floor, north wall, west wall, or east wall) each projected window corner point fell. These variables were then used to direct program execution to the proper section. Since this model was written in Fortran IV programming language, computed GO TO statements were used. This type of statement transfers control of the program to different locations, depending on the value of a variable (i.e. the aforementioned variables). Execution of the subroutine was transferred through a set of 17 computed GO TO statements. The first statement transferred control to various other GO TO statements as a function of the location of B_p. These statements, in turn, transferred

Table B.1 Possible Configurations of the Sunlit Areas

Configuration	Location of			
	A_p	B_p	C_p	D_p
1	floor	floor	floor	floor
2	floor	floor	west wall	floor
3	floor	floor	west wall	west wall
4	north wall	north wall	north wall	north wall
5	floor	north wall	north wall	floor
6	floor	north wall	west wall	floor
7	floor	north wall	west wall	west wall
8	north wall	north wall	west wall	west wall
9	floor	west wall	west wall	floor
10	floor	west wall	west wall	west wall
11	west wall	west wall	west wall	west wall
12	floor	east wall	north wall	floor
13	east wall	east wall	north wall	floor
14	east wall	east wall	north wall	north wall
15	floor	east wall	floor	floor
16	east wall	east wall	floor	floor
17	floor	east wall	east wall	floor
18	east wall	east wall	east wall	floor
19	east wall	east wall	east wall	east wall

control as a function of another projected point. This procedure was repeated until the proper case was reached. For example, if B_p fell on the floor (A_p must also fall on the floor), the next statement checked the location of C_p, and the following statements checked the location of D_p.

As a check on this method, the subroutine contained an error message which was printed if the sunlit area configuration did not match one of the 19 allowable ones. The error message was never encountered during any run, indicating that all of the possible configurations are contained in Table B.1. The possibilities were derived using physical reasoning and the inherent physical limitations of the system.

APPENDIX C

DIFFERENTIAL ELEMENT VIEW FACTORS

The method which was used in the direct gain model to calculate the diffuse radiation view factors necessitated expressions for view factors from differential elements to planar surfaces. Equations were needed for two configurations, perpendicular surfaces and parallel surfaces. The equations were derived from expressions obtained from Seigel and Howell [21].

Figure 3.1 illustrates a differential element, dA_1, which is perpendicular to surface A_2. The element lies in a plane which intersects A_2 along its bottom edge. Using the nomenclature given in the figure, the view factor from dA_1 to A_2, F_{d1-2}, is given by

$$F_{d1-2} = \frac{1}{2\pi}\left\{\tan^{-1}\left(\frac{w-y}{x}\right) + \tan^{-1}\left(\frac{y}{x}\right) - \frac{x}{\sqrt{x^2 + y^2}}\left[\tan^{-1}\left(\frac{w - y}{\sqrt{h^2 + x^2}}\right) + \tan^{-1}\left(\frac{y}{\sqrt{h^2 + x^2}}\right)\right]\right\} . \qquad (C.1)$$

Figure C.2 illustrates a differential element which lies in a plane parallel to surface A_2. The expression for F_{d1-2} was found by summing the view factors from the element to each section of A_2 (a, b, c, and d). The terms were then regrouped, resulting in

$$F_{d1-2} = \frac{1}{2\pi s}\left[\begin{array}{l}
\dfrac{x}{\sqrt{1+(x/s)^2}}\left(\tan^{-1}\dfrac{y/s}{\sqrt{1+(x/s)^2}} + \tan^{-1}\dfrac{(h-y)/s}{\sqrt{1+(x/s)^2}}\right) + \\
\dfrac{w-x}{\sqrt{1+(\frac{w-x}{s})^2}}\left(\tan^{-1}\dfrac{y/s}{\sqrt{1+(\frac{w-x}{s})^2}} + \tan^{-1}\dfrac{(h-y)/s}{\sqrt{1+(\frac{w-x}{s})^2}}\right) + \\
\dfrac{y}{\sqrt{1+(y/s)^2}}\left(\tan^{-1}\dfrac{x/s}{\sqrt{1+(y/s)^2}} + \tan^{-1}\dfrac{(w-x)/s}{\sqrt{1+(y/s)^2}}\right) + \\
\dfrac{h-y}{\sqrt{1+(\frac{h-y}{s})^2}}\left(\tan^{-1}\dfrac{x/s}{\sqrt{1+(\frac{h-y}{s})^2}} + \tan^{-1}\dfrac{(w-x)/s}{\sqrt{1+(\frac{h-y}{s})^2}}\right)
\end{array}\right] \qquad \text{(C.2)}$$

Equations (C.1) and (C.2) were used in conjunction with Equation (2.2) to calculate the diffuse radiation view factor for each pair of heat transfer surfaces within the direct gain system.

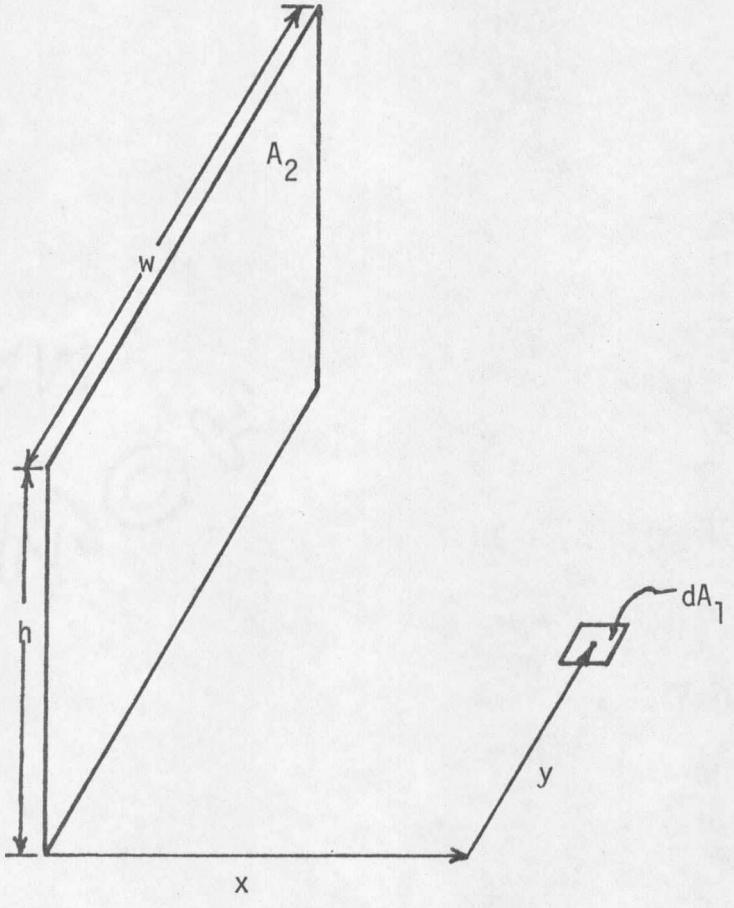


Figure C.1 Differential Element for Perpendicular Surfaces

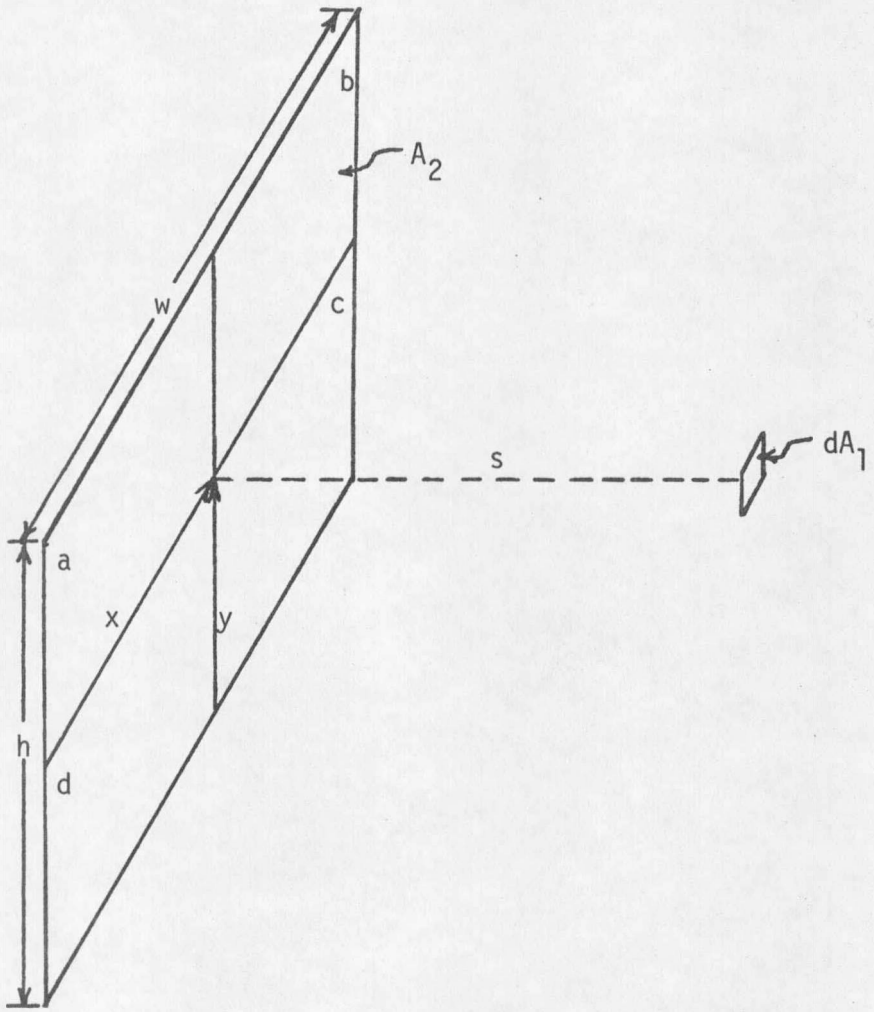


Figure C.2 Differential Element for Parallel Surfaces

APPENDIX D

NUMERICAL DOUBLE INTEGRATION

In order to calculate the diffuse radiation view factor for each pair of heat transfer surfaces within the direct gain model, as presented in Chapter II, a method for performing numerical double integration was needed. Such methods appear in many numerical methods texts. The method which was used is very similar to, but was developed independently from, that presented by Gerald [22]. The technique which follows is applicable to any numerical integration method. Simpson's method was used for this development because it is the most commonly used numerical integration method.

Suppose the integral, I, of the function F(x,y) is desired, defined as

$$I = \int_{y_0}^{y_m} \int_{x_0}^{x_n} F(x,y)dxdy. \qquad (D.1)$$

This equation may be rewritten as

$$I = \int_{y_0}^{y_m} G(y)dy \qquad (D.2)$$

where

$$G(y) = \int_{x_0}^{x_n} F(x,y)dx. \qquad (D.3)$$

Using a Simpson's rule integration, Equation (D.2) may be approximated as

$$I \doteq \frac{\Delta y}{3} [G(y_0) + 4G(y_1) + 2G(y_2) + 4G(y_3) + 2G(y_4) + \ldots$$

$$+ 4G(y_{m-3}) + 2G(y_{m-2}) + 4G(y_{m-1}) + G(y_m)] \qquad (D.4)$$

where

$$G(y_i) = \int_{x_0}^{x_n} F(x,y_i)dx. \qquad (D.5)$$

However, $G(y_i)$ may also be approximated, using Simpson's rule, as

$$G(y_i) \doteq \frac{\Delta x}{3} [F(x_0,y_i) + 4F(x_1,y_i) + 2F(x_2,y_i) + \ldots$$

$$+ 2F(x_{n-2},y_i) + 4F(x_{n-1},y_i) + F(x_n,y_i)]. \qquad (D.6)$$

Numerical double integration may thus be performed by using Equation (D.4), with each term determined from Equation (D.6).

APPENDIX E

INSOLATION AND AMBIENT TEMPERATURE DATA GENERATION

As explained in Chapter II, the various passive solar system models used to perform this study could only be run with hourly or sub-hourly insolation and ambient temperature data. Actual measured hourly insolation data were not available for Bozeman, Montana. They are available for Great Falls, Montana, but the extrapolation of this data to Bozeman could result in large errors, due to significant elevation and climatic differences between the two locations. Average daily insolation values, however, are available for Bozeman. The necessary sub-hourly insolation data were generated such that they satisfied the average conditions. The insolation was assumed to be distributed throughout the day in a sinusoidal form, as shown in Figure E.1. The general equation for the insolation distribution, q_s, of this form is (for daylight hours)

$$q_s = q_{ave}\left(1 - \cos\frac{2\pi(t-SR)}{DL}\right). \qquad (E.1)$$

The total insolation for the day, H_s, is given by

$$H_s = \int_0^{24} q_s dt = \int_{12-\frac{DL}{2}}^{12+\frac{DL}{2}} q_s dt. \qquad (E.2)$$

Equation (E.1) was substituted into (E.2), the integration was performed and q_{ave} was found to be

$$q_{ave} = \frac{HS}{DL}. \qquad (E.3)$$

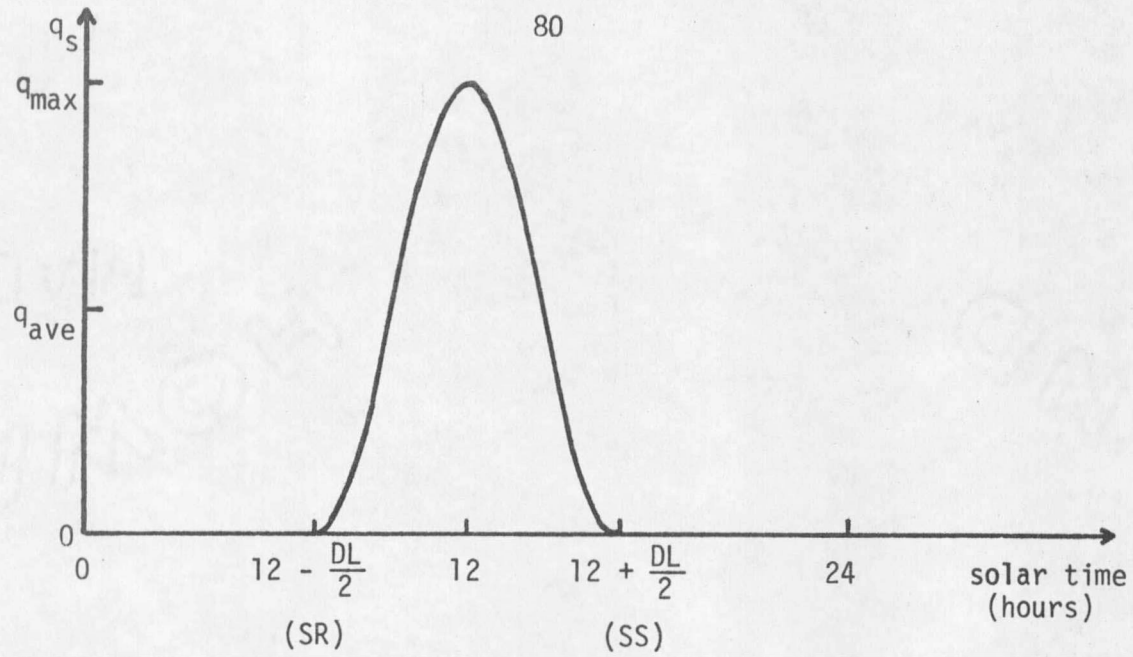


Figure E.1 The Assumed Insolation Distribution

The necessary sub-hourly insolation data were thus generated using

$$q_s = \frac{HS}{DL}\left(1 - \cos\frac{2\pi(t-SR)}{DL}\right); \quad SR \leq t \leq SS$$

$$= 0 \text{ at night.} \qquad \text{(E.4)}$$

The day length, DL, was calculated using relations obtained from Duffie and Beckman [14]. It is a function only of the day of the year and of the latitude of the test location.

Hourly ambient temperature data are available for Bozeman, as they are for any U.S. Weather Service recording station. These data were not used directly, because a specific number of heating degree days and nights were desired for the test case ambient temperature distribution.

Heating degree days, DD, are defined as

$$DD = \text{heating degree days (for one day)}$$

$$= \frac{1}{24} \int_{12-\frac{DL}{2}}^{12+\frac{DL}{2}} (T_{ref} - T_{amb})dt \qquad (E.5)$$

where T_{ref} = reference temperature = 18.3°C (65°F).

Degree nights, DN, are defined the same, except that the integration is performed only for nighttime ambient temperatures. The hourly ambient temperature data which were available were used to determine the average total monthly heating degree days and nights for Bozeman (from 1968 to 1977). These values are listed in Table E.1. The sum of degree days and nights equals conventional degree days, DD_{conv}.

The simulations which were performed for this study used ficticious (hypothetical) ambient temperature data. The temperature distribution was assumed to be sinusoidal in form, as shown in Figure E.2. The general equation for this distribution is

$$T_{amb} = T_{mean} - (T_{max} - T_{mean}) \cos \frac{\pi t}{12}. \qquad (E.6)$$

The distribution was also constrained to have a number of heating degree days and nights equal to the daily average for January in Bozeman, as determined from Table E.1. Degree days are defined by Equation (E.5).

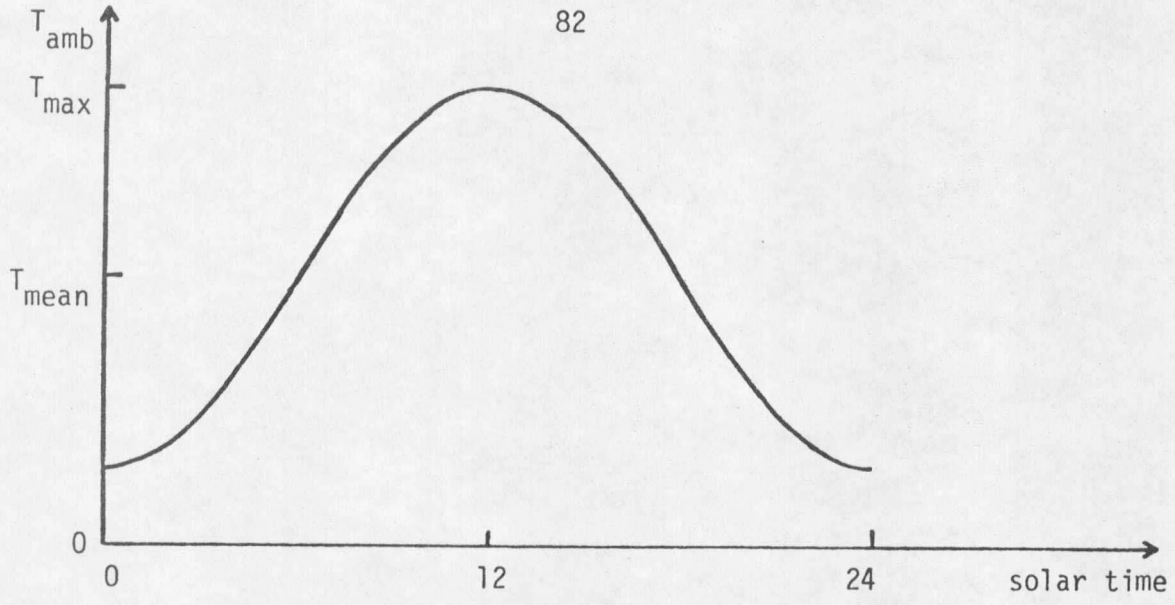


Figure E.2 The Assumed Ambient Temperature Distribution

Conventional degree days are defined as

$$DD_{conv} = DD + DN = \int_0^{24} (T_{ref} - T_{amb})dt. \qquad (E.7)$$

Equation (E.6) was substituted into (E.5) and the integration was performed, resulting in

$$DD = T_{ref}\frac{DL}{24} + T_{mean}\left(\frac{1}{\pi}\sin\frac{\pi DL}{24} - \frac{DL}{24}\right) - T_{max}\frac{1}{\pi}\sin\frac{\pi DL}{24}. \qquad (E.8)$$

Equations (E.6) and (E.8) were then substituted into (E.7) and the integration was performed, resulting in

$$DN = T_{ref}\left(1 - \frac{DL}{24}\right) + T_{mean}\left[\frac{DL}{24} - \frac{1}{\pi}\sin\frac{\pi DL}{24} - 1\right] +$$

$$T_{max}\frac{1}{\pi}\sin\frac{\pi DL}{24}. \qquad (E.9)$$

Table E.1 Degree Day/Night Averages for Bozeman, Montana (1968-1977)

Month	Degree Days °C	Degree Nights °C
January	265	567
February	228	413
March	250	361
April	190	230
May	127	141
June	66	79
July	31	46
August	32	57
September	78	147
October	134	277
November	173	405
December	235	522

Equations (E.8) and (E.9) were solved simultaneously for T_{mean} and T_{max}, resulting in

$$T_{mean} = T_{ref} - (DD + DN) \tag{E.10}$$

and

$$T_{max} = \frac{\pi}{\sin \frac{\pi DL}{24}} \left[T_{ref} \frac{DL}{24} + (T_{ref} - DD - DN)\left(\frac{1}{\pi}\sin\frac{\pi DL}{24} - \frac{DL}{24}\right) - DD \right] \tag{E.11}$$

The necessary sub-hourly ambient temperature data were then generated

using Equation (E.6), with T_{mean} and T_{max} determined from Equations (E.10) and (E.11). The data then had the required number of heating degree days and nights.

LITERATURE CITED

LITERATURE CITED

1. Stromberg, R. P. et al, Passive Solar Buildings: A Compilation of Data and Results, Sandia Laboratories publication SAND 77-1204, 1977.

2. Trombe, F., "Heating by Solar Radiation," CNRS Internal Report B-1-73-100, 1973.

3. Balcomb, J. D., J. C. Hendstrom, and R. D. McFarland, "Passive Solar Heating of Buildings," Los Alamos Scientific Laboratories publication LA-UR-77-1162, 1977.

4. Bilgen, E. and R. Jeldres, On the Optimization of Trombe Wall Solar Collectors, American Society of Mechanical Engineers publication 78-WA/SOL-13, 1978.

5. Ohanessian, P. and W. W. S. Charters, "Thermal Simulation of a Passive Solar House Using a Trombe-Michel Wall Structure," Solar Energy, vol. 20, pp. 275-281, 1978.

6. Palmiter, L., T. Wheeling, and B. Corbett, "Measured and Modeled Passive Performance in Montana," International Solar Energy Society Annual Meeting, Denver, Colorado, proceedings, 1978.

7. Emery, A. F., C. J. Kippenhan, D. R. Heerwagen, and G. B. Varey, The Simulation of Building Heat Transfer for Passive Solar Systems, American Society of Mechanical Engineers publication 79-WA/SOL-38, 1979.

8. Balcomb, J. D., R. D. McFarland, and S. W. Moore, "Passive Testing at Los Alamos," 2nd National Passive Solar Conference, Philadelphia, proceedings, 1978.

9. Palmiter, L., T. Wheeling, and B. Corbett, "Performance of Passive Test Units in Butte, Montana," National Center for Appropriate Technology (NCAT), Butte, Montana, 1978.

10. Balcomb, J. D., and R. D. McFarland, "A Simple Empirical Method for Estimating the Performance of a Passive Solar Heated Building of the Thermal Storage Wall Type," 2nd National Passive Solar Conference, Philadelphia, proceedings, 1978.

11. Warrington, R. O., R. E. Stotts, R. L. Mussulman, and W. R. Martindale, "A New and Simple Method for Estimating the Monthly and Yearly Performance of Passive Solar Systems," International Solar Energy Conference, Atlanta, proceedings, 1979.

12. Wray, W. O., and J. D. Balcomb, "Trombe Wall vs. Direct Gain: A Comparative Analysis of Passive Solar Heating Systems," 3rd National Passive Solar Conference, San Jose, California, proceedings, 1979.

13. Noll, J. A., J. F. Roach, and S. Ben-David, "Trombe Walls and Direct Gain: Patterns of Nationwide Applicability," ibid.

14. Duffie, J. A., and W. A. Beckman, Solar Energy Thermal Processes, New York: John Wiley & Sons, 1974.

15. Holman, J. P., Heat Transfer, fourth edition, New York: McGraw-Hill, 1976.

16. Hottel, H. C., and A. F. Sarofim, Radiative Transfer, New York: McGraw-Hill, 1967.

17. ASHRAE Handbook of Fundamentals, New York: American Society of Heating, Refrigerating and Air-Conditioning Engineers, Inc., 1977.

18. Carnahan, G., H. A. Luther, and J. O. Wilkes, Applied Numerical Methods, New York: John Wiley & Sons, 1969.

19. Wadsworth, B., and L. Palmiter, "A Radiation Shield for Air Temperature Measurement," Solar '79 Northwest Conference, Seattle, Wash.

20. Busch, R. D., Reduction and Publication of Passive Solar Data, volume II: "Passive Solar Data From the National Center for Appropriate Technology," Bickle/CM, Albuquerque, New Mexico, 1979.

21. Siegel, R., and J. R. Howell, Thermal Radiation Heat Transfer, New York: McGraw-Hill, 1972.

22. Gerald, C. F., Applied Numerical Analysis, Reading, Massachusetts: Addison-Wessley, 1970.

MONTANA STATE UNIVERSITY LIBRARIES
3 1762 10015584 3

[redacted]

N378
St77
cop.2

Stotts, Robert E
Modeling and comparisonof passive solar heating systems

DATE	ISSUED TO
APR 8	C. LOFGREN 416 W. OLIVE APT [redacted]

[redacted]

N378
St77
cop 2